SOX2 reprograms the methionine cycle by RMST-conferred AHCY sequestration in cancer

Author Information

Iqra Ishrat[1,2+], Zafar Iqbal Bhat[2,3+], Zhihua Guo[4+], Hilary K. Ho[1,2], Ruiqi Ma[2], Qing Tang[5,6], Jinghao Liang[4], Yanxi Huang[5,6], Lei Zhang[1,2], Yung Hou Wong[5,6], Nada Jabado[7], Weiqiang Yin[4]*, Hong Kee Tan[8]*, Justin L. Tan[2,9]*

[1]School of Chemical Biology and Biotechnology, Shenzhen Graduate School, Peking University, Shenzhen, 518055, China

[2]Institute of Cancer Research, Shenzhen Bay Laboratory, Shenzhen, 518132, China

[3]School of Life Sciences, University of Science and Technology of China, Hefei, 230027 China

[4]Department of Thoracic Surgery and Oncology, the First Affiliated Hospital of Guangzhou Medical University. State Key Laboratory of Respiratory Disease & National Clinical Research Center for Respiratory Disease, Guangzhou 510120, China

[5]Division of Life Sciences and the Biotechnology Research Institute, Hong Kong University of Science and Technology; Hong Kong, 999077, China

[6]State Key Laboratory of Molecular Neuroscience and the Molecular Neuroscience Center, Hong Kong University of Science and Technology; Hong Kong, 999077, China

[7]Department of Pediatrics, McGill University Health Centre, Montréal, Quebec, Canada

[8]Paediatric Bone Marrow Transplantation and Cell Therapy Centre, Children's Blood and Cancer Centre, KK Women's and Children's Hospital, SingHealth, Singapore, Singapore.

[9]School of Basic Medical Science, Capital Medical University, Beijing, 100069, China.

+Equal contribution.

***Corresponding authors.**

Email: justintanlab@gmail.com, tan.hong.kee@kkh.com.sg, yinweiqiang88@163.com

Abstract

Transcription factors drive gene expression dysregulation in cancer. However, non-canonical oncogenic mechanisms of these factors are unclear. Utilizing function-centric proteomics to discover RNA-dependent protein-protein interactions, we

uncovered an unexpected interaction between transcription factor oncogene SOX2 and methionine cycle enzyme AHCY. Immunofluorescence and CUT&RUN revealed that SOX2 expression sequesters AHCY to the chromatin. A candidate RNA-immunoprecipitation screen identified non-coding RNA RMST as a mediator of the SOX2 and AHCY interaction. The SOX2-AHCY interaction is reduced upon RMST knockdown. SOX2 expression sequesters RMST and AHCY in the nucleus, an activity dependent on the RNA-binding Arginine Rich Motif (ARM) domain of SOX2. Metabolite profiling revealed that SOX2 expression alters methionine cycle intermediates, particularly at the AHCY catalyzed step. Methylation precursor S-adenosylmethionine (SAM) production is also inhibited by SOX2. These metabolic changes are rescued with SOX2 ARM mutation. Whole genome bisulfite sequencing revealed that SOX2 expression induces DNA hypomethylation in cancer cells. DNA hypomethylation and its downstream DNA damage effect are rescued with SAM supplementation or SOX2 ARM mutation. These data suggest that SOX2 mis-expression in cancer sequesters AHCY, through an RMST adaptor, in the nucleus. This reduces the availability of cytoplasmic AHCY to participate in the methionine cycle, reprograming this metabolic process. As a result, SAM levels are reduced, causing DNA hypomethylation and downstream DNA damage. Our findings were validated in cancer patient biopsies. Strikingly, knockdown and pharmacological inhibition of AHCY targets SOX2-expressing cancer cells in culture and *in vivo*. This suggests that low SAM levels, induced by decreased cytoplasmic AHCY, sensitize SOX2-expressing cancer cells to AHCY inhibition. Overall, our results suggest that a transcription factor can coopt a non-coding RNA to perform non-canonical metabolic reprograming, creating a druggable metabolic dependency in transcription factor-driven cancer.

Graphical Abstract

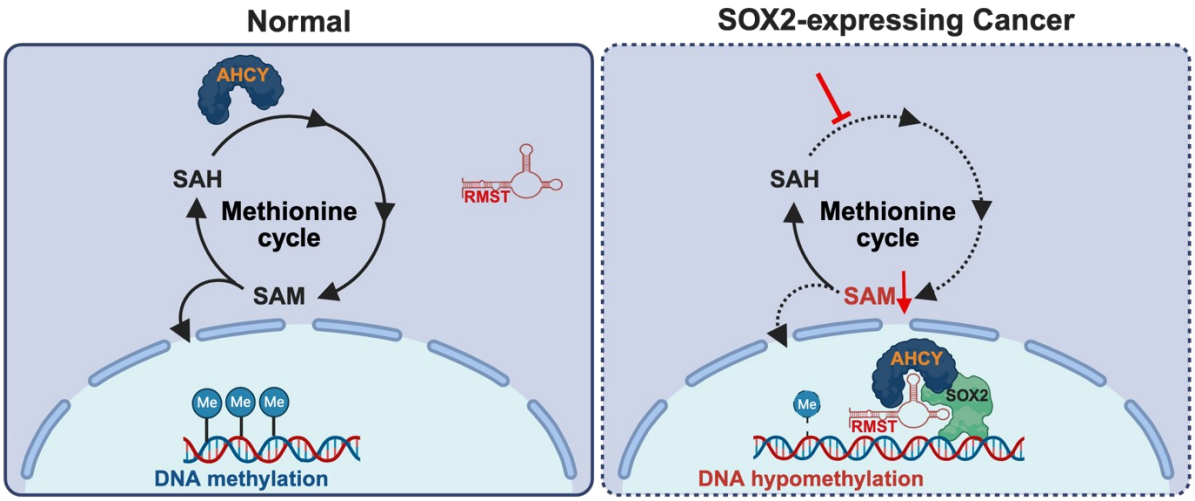

In normal cells, cytoplasmic AHCY drives the methionine cycle to generate sufficient SAM for homeostatic DNA methylation. In cancer, SOX2 is mis-expressed, sequestering AHCY in the nucleus through an RMST adaptor. The decrease in cytoplasmic AHCY inhibits the methionine cycle, resulting in less SAM generation. This in turn induces DNA hypomethylation in cancer.

Introduction

RNA-protein interactions are key drivers of many cellular processes such as translation, epigenetic modification, mRNA splicing, and nuclear-cytoplasmic shuttling, with dysregulation implicated in disease [1,2]. Methods developed to identify and study RNA-protein interactions have been limited to RNA-centric or protein-centric techniques [3]. RNA-centric methods involve the use of RNA probes that are cross-linked to bound proteins either *in vitro* or *in vivo* [4,5]. Bound proteins are then purified for downstream analyses. Protein-centric methods involve cellular cross-linking of RNA and protein followed by immunoprecipitation of RNA-protein complexes with antibodies specific to proteins-of-interest [6]. Bound RNA is purified for downstream analysis. Current approaches to identify RNA-protein interactions primarily assess the binding of RNA to protein without any information on the functional relevance of the interaction. Downstream characterization is required to determine the biological significance of interactions, and in some studies, specific mechanisms are not well defined. A function-centric method to identify RNA-protein

interactions could increase the rate of biologically meaningful discoveries and aid in defining precise mechanisms of these interactions.

Studies have showcased the roles that RNA-protein interactions play in cancer [7,8]. There are some notable examples with defined mechanisms. Transcription factor (TF) p53 has been shown to transcriptionally upregulate the large intergenic non-coding RNA lincRNA-p21 to form a complex with hnRNP-K protein, suppressing oncogene expression [9]. HOTAIR lncRNA interacts with PRC2 to promote cancer invasiveness and metastasis [10]. The HEXIM1 TF binds and stabilizes transcripts of tumour suppressor genes to suppress melanoma [11]. With the close proximity of TFs to transcribed RNA in the nucleus, uncovering functional TF-RNA interactions could potentially lead to new discoveries in RNA-protein biology.

A viable target to study oncogenic TF-RNA interactions is the transcription factor TF SOX2. SOX2 is aberrantly upregulated in at least 15 different cancers and plays important roles in various aspects of cancer pathogenesis [12]. Normally, SOX2 is crucial in the regulation of pluripotency, differentiation, and development [13]. However, the exact molecular mechanisms by which SOX2 supports tumorigenesis are not well defined [14]. Interestingly, SOX2 has been shown to bind RNA [15]. SOX2 interacts with long non-coding RNA (lncRNA) RMST to regulate neurogenesis, pluripotency, brain development, and neural differentiation in mouse embryonic stem cells (mESCs) [16]. In human embryonic stem cells (hESCs), the ES lncRNA family binds SOX2 and the polycomb repressor complex 2 (PRC2) to regulate pluripotency [17]. It is currently unclear how SOX2 interacts with RNA in cancer.

The methionine cycle plays an essential role in major homeostatic processes such as purine biosynthesis, polyamine metabolism, and methylation reactions [18]. An important methionine cycle product is SAM, a metabolite essential for DNA [19], RNA, and histone methylation [20]. The methionine cycle has been implicated in cancer[18,21]. For instance, Polyamine sythesis, mediated by the methionine cycle, is required for pancreatic cell proliferation [22]. Drugging the methionine cycle enzyme MAT2A targets lung tumor initiating cells [23]. Imbalance in methionine metabolism triggers tumor suppressor p53 inactivation in many cancer types, inducing downstream genomic instability [24]. Other then canonical gene expression regulation, little is known about non-transcriptional regulation of the methionine cycle by TFs.

To enable function-centric discovery of RNA-TF interactions, we developed Surveying the Protein RNA-dependent Interactome (SPRINT). SPRINT involves the co-immunoprecipitation (co-IP) of a target protein-of-interest and proteomic determination of its protein binders in the presence or absence of RNase. This uncovers RNA-dependent alterations in the composition of a protein complex as a proxy for infering functional RNA-protein interactions. Here, we applied SPRINT to identify RNA-dependent protein partners of SOX2 in small cell lung cancer (SCLC). Unexpectedly, we identified methionine cycle enzyme AHCY as an RNA-dependent SOX2 protein partner. We demonstrated that in small cell lung cancer (SCLC) and hepatocellular carcinoma (HCC) cells, SOX2 expression is correlated with nuclear sequestration of AHCY by immunofluorescence (IF). A SOX2 gain of function (GOF) cell line showed nuclear sequestration of AHCY. CUT&RUN revealed AHCY enrichment at chromatin upon SOX2 expression. Through a candidate lncRNA RNA-immunoprecipitation (RIP) screen, we identified lncRNA RMST as a binder of both SOX2 and AHCY. RMST knockdown revealed that SOX2-expressing cancer cells are dependent on RMST for survival. In addition, RMST knockdown reduced the co-immunoprecipitation (Co-IP) of SOX2 with AHCY. SOX2 expression sequesters RMST and AHCY in the nucleus, an activity dependent on the RNA-binding ARM domain of SOX2. Our results suggest that SOX2 sequesters AHCY in the nucleus through an RMST adaptor.

Since AHCY is a metabolic enzyme, we studied the effects of SOX2 expression on metabolism. Metabolite profiling revealed that SOX2 expression significantly alters methionine cycle metabolites, particularly at the AHCY catalyzed step. In addition, methylation precursor SAM is significantly downregulated by SOX2 expression. Methionine cycle alterations by SOX2, including low SAM, are rescued by mutations of the SOX2 ARM (RNA-binding) domain. Since SAM is a key precursor for DNA methylation, we examined the effects of SOX2 expression on DNA methylation. Whole genome bisulfite sequencing (WGBS) revealed global DNA hypomethylation in SOX2-expressing cancer cells. Chromosomal instability markers were also upregulated by SOX2 expression. Interestingly, DNA hypomethylation and DNA damage markers were rescued by SAM supplementation and SOX2 ARM mutation. We validated these findings in SCLC patient biopsies. These data suggest that the SOX2-RMST-AHCY sequestration complex inhibits the methionine cycle. This

decreases SAM levels, resulting in the cancer hallmarks of global DNA hypomethylation and chromosomal instability.

As our proposed SOX2-mediated oncogenic mechanism reprograms the methionine cycle to lower SAM levels, we explored if further inhibiting AHCY would be detrimental to cancer cell survival. We showed that SOX2-expressing cancer cells are particularly susceptible to AHCY knockdown. Strikingly, pharmacological inhibition of AHCY via small molecule inhibitor 3-deazaneplanocin A (DZNep) markedly decreased SOX2-high cancer cell viability and caused significant tumor regression in SOX2-driven orthotopic SCLC xenografts. Our findings suggest an unexpected mechanism of a transcription factor utilizing non-coding RNA to achieve metabolic reprograming in cancer. In addition, this mechanism proposes a specific metabolic vulnerability that can be drugged to treat SOX2-driven cancers.

Results

SPRINT identifies RNA-dependent SOX2 protein complexes

To study SOX2-RNA interactions in SCLC, we first validated that SOX2 is functionally relevant in cell line models. We obtained two SCLC cell lines with undetectable levels of SOX2 (SOX2 lo), DMS114 and SW1271 and two endogenous SOX2-expressing (SOX2 hi) cell lines, H69 and H446 (Figs. S1A and S1B). Since these cell lines are genetically dissimilar, we developed a SOX2 gain of function (GOF) line by expressing SOX2 in the DMS114 SOX2 lo cell line, DMS114 *Tg:SOX2*, and created an accompanying empty vector control, DMS114 EV (Figs. S1A and S1B). The isogenic GOF cell line allowed us to investigate phenomenon specific to SOX2, unaffected by genetic differences when comparing the endogenous cell lines. To validate the importance of SOX2 in SCLC cells, we knocked down SOX2 in the aforementioned 6 cell lines (Figs. S1C-S1J). SOX2 knockdown selectively reduced the cell viability of SOX2 hi cells, leaving SOX2 lo cells unaffected (Figs. S1E-S1J). Interestingly, the SOX2 GOF cell line was also affected by SOX2 knockdown, indicating that ectopic SOX2 expression in a previously SOX2-independent cell line could induce SOX2-dependency (Figs. S1I and S1J). These results suggest that SOX2, when amplified or overexpressed, is crucial for SCLC cell viability.

After cell line model validation, we optimized the steps required for SPRINT. SPRINT involves co-IP of a protein-of-interest with its protein complex members, in the absence and presence of RNase treatment. The two conditions are then subjected to mass spectrometry (MS) analysis to identify changes in binding proteins in the absence of RNA (Fig. 1A). We first treated H446 cell lysate with varying amounts of RNase to identify the optimal concentration needed to remove the majority of cellular RNAs in the co-IP reactions (Fig. S1K). Next, we selected H69 and DMS114 *Tg:SOX2* cells for SOX2 SPRINT. This selection of an endogenous SOX2 hi and SOX2 GOF cell line allows us to identify overlapping hits, which are likely biologically relevant and specific to SOX2 functioning. We validated that our chosen SOX2 antibody could specifically pull down SOX2 in both H69 and DMS114 *Tg:SOX2* via western blot (Fig. S1L).

SPRINT was then performed to generate three lists of proteins per cell line: proteins non-specifically pulled down by IgG control antibody, proteins pulled down by SOX2 co-IP, and proteins pulled down by SOX2 co-IP with RNase treatment (Fig. 1B). Unlike other RNA-protein interaction detection methods, SPRINT does not involve an RNA-protein cross-linking step, which minimizes non-specific binding. We focused on proteins that bound SOX2 but were not detected in IgG and RNase treated conditions above our cutoffs. This implied that these proteins were specifically bound to SOX2, with their binding lost upon RNase treatment. We identified 246 such proteins in H69 and 139 such proteins in DMS114 *Tg:SOX2* (Fig. 1B). Overlapping these proteins resulted in a list of 20 proteins in common between the two cell lines (Table S1). These proteins had low abundance in the IgG and RNase-treated conditions relative to the SOX2 pulldown condition (Fig. 1C). We also verified that SOX2 pulldown efficiency was unaffected by RNase treated, as reflected by similar SOX2 protein abundance in both SOX2 pulldown and RNase conditions (Fig. 1C). Our results suggest that SPRINT robustly identifies RNA-dependent protein binders of SOX2.

Interestingly, we noticed significant SPRINT enrichment of 7 protein synthesis associated proteins as RNA-dependent SOX2 binders (Fig. 1C and Table 1). IARS1, HARS1, and LARS1 are aminoacyl-tRNA synthetases that link tRNAs to their cognate amino acids [25]. RPLP0, RPLP1, and RPLP2 are integral ribosomal protein subunits

[26,27]. RBM3 is a ribosomal binding protein that enhances protein synthesis [28]. Since the ribosome consists of both RNA and protein, our data suggests that SOX2 interacts with the ribosome in an RNA-dependent manner. This finding posits an intriguing possibility of SOX2 regulating both transcription and translation in cell fate determination and disease, a finding which was recently independently validated [29]. With other interesting non-transcriptional pathways being implicated as co-dependent on SOX2 and RNA (Fig. 1C and Table 1), we propose that SPRINT is a useful, generalizable method to discover novel RNA-protein biology for other proteins of interest.

SOX2 interacts with AHCY in an RNA-dependent manner

We were particularly interested in RNA-dependent SOX2 binder AHCY because of its unusual subcellular localization in SOX2 hi cells. AHCY performs its primary function as a methionine cycle enzyme in the cytoplasm. However, when we performed co-immunofluorescence (co-IF) to validate SOX2 and AHCY co-localization, we noticed that in SOX2 expressing SCLC cells, AHCY was primarily present in the nucleus (Fig. 1D). Conversely in SOX2 lo SCLC cells, AHCY was observed in both the nucleus and cytosol (Fig. 1D). We made a similar observation in SOX2 hi and lo HCC cells (Fig. S1B), suggesting the generalizability of these results (Fig. 1E). Similar nuclear localization enhancement was observed in the SOX2 GOF cells (Figs. 1D and 1F). SPRINT data showed that the association of AHCY with SOX2 decreased by ~50% upon RNase treatment (Figs. S2A and S2B), with minimal differences in SOX2 levels with or without RNase treatment (Figs. S2C and S2D). We validated our SPRINT data on AHCY by co-IP Western blot, which showed a similar decrease in AHCY binding to SOX2 upon RNase treatment (Figs. S2E-S2G).

Since SOX2 is canonically a TF that binds chromatin, we examined if SOX2 sequesters AHCY to the chromatin via CUT&RUN qPCR [30]. We designed primers to the promoter regions of several genes where SOX2 showed enrichment in published chromatin immunoprecipitation experiments [16]. We found that AHCY and SOX2 showed co-enrichment at several chromatin binding sites in SOX2 hi and SOX2 GOF cells (Figs. 1G and 1H). In SOX2 lo cells, AHCY was not enriched at any chromatin sites (Fig. 1I). We observed that AHCY mRNA expression was similar across SCLC and HCC cell lines regardless of their SOX2 expression level (Figs. S2H and S2I).

This validated that AHCY was not affected by SOX2 at the transcriptional level. Our results suggest that SOX2 sequesters AHCY at chromatin in an RNA-dependent manner.

SOX2-AHCY binding is conferred by lncRNA RMST

To identify the RNAs responsible for the SOX2-ACHY interaction, we performed RNA immunoprecipitation (RIP), without RNA-protein cross-linking, followed by qRT-PCR detection of candidate transcripts. We probed for several lncRNA candidates previously found to be bound by SOX2 in hESCs [17], by AHCY in the human embryonic kidney HEK293 cell line [31], or with functional implications in cancers [10,32,33]. Among these candidates, H19, HOTAIR, and LincROR had near undetectable expression in SOX2 hi and SOX2 GOF cells (Figs. 2A, 2B, S3A-S3C). ES1, ES2, and PVT1 showed significantly lower, albeit detectable, levels in SOX2 hi and SOX2 GOF cells (Figs. 2A, 2B, S3D-S3F). Conversely, the major RMST isoform (AK056164) and ES3 were expressed in SOX2 hi and GOF cells (Figs. 2A, 2B, S3G, S3H). Interestingly, their expression positively correlated with SOX2 expression (Figs. 2A and 2B). We assessed the binding of ES1, ES2, ES3, PVT1, and RMST to SOX2 and AHCY in RIP experiments. Strikingly, we observed significant levels of only ES3 and RMST lncRNAs bound by SOX2 and AHCY (Fig. 2C).

Next, we assessed the functional roles of ES3 and RMST in SOX2 hi SCLC. *ES3* knockdown (Figs. S3I, S3J) had minimal effect on the cell viability of both DMS114 EV and SOX2 GOF cells (Figs. S3K and S3L). However, *RMST* knockdown selectively reduced the cell viability of SOX2 hi and SOX2 GOF SCLC cells (Figs. 2D-2G). Similarly, SOX2 hi HCC cells were sensitive to *RMST* knockdown while there was little effect on SOX2 lo cells (Figure 2H-2K). Since only RMST demonstrated a role in SOX2-expressing cell viability, we further validated its interaction with SOX2 and AHCY. We synthesized biotinylated RMST and antisense RMST transcript (AS RMST) to perform protein pulldown. Our RMST bait successfully pulled down both SOX2 and AHCY in SOX2 hi H446 and SOX GOF cell lysates, with no pulldown observed in AS RMST and the no RNA bait conditions (Figs. 2L and 2M). In addition, *RMST* knockdown reduced the amount of AHCY bound to SOX2 in Co-IP (Fig. 2N). We validated that this loss of AHCY signal was not due to a decrease in cellular AHCY, or SOX2 mRNA or protein levels due to *RMST* knockdown (Figs. S3M and

S3N). Examining the LncExpDB database [34] revealed that RMST is significantly upregulated in SCLC, although minimal upregulation is observed in liver cancer (Fig. 2O). Our results suggest that RMST plays an important role in cancer cell viability by conferring the SOX2-AHCY interaction.

SOX2 sequesters RMST and AHCY in the nucleus through its RNA-binding domain

To further understand the role of the SOX2-RMST-AHCY complex in cancer, we examined the cellular localization of RMST to provide more mechanistic clues. We performed RNA fluorescence *in situ* hybridization (RNA-FISH) and found that in SOX2 lo DMS114 EV cells, RMST was present in both the nucleus and cytoplasm. However, in SOX2 GOF cells, RMST localized predominantly to the nucleus, similar to what we observed for AHCY (Figs. 1D-F and 3A). It has been reported that SOX2 TF binds to RNA via its Arginine Rich Motif (ARM) domain [35]. To validate that RMST nuclear sequestration is through direct SOX2 binding, we mutated the ARM domain of SOX2 (Fig. 3B). Wildtype SOX2 expression in SOX2 lo DMS114 and SW1271 cell lines induced RMST nuclear sequestration, while ARM-mutant SOX2 expression abrogated this effect, with the majority of RMST present in the cytoplasm (Figs. 3C and 3D). This suggests that SOX2 sequesters RMST in the nucleus via its RNA-binding domain.

To further validate the differences in RMST localization in SOX2 hi and lo cells, we performed nuclear-cytoplasmic fractionation followed by qPCR in the DMS114 EV and SOX2 GOF cell lines. We used HPRT and MALAT1 transcripts as cytoplasmic and nuclear markers respectively [36]. The expression of both HPRT and MALAT1 RNA corresponded to their respective cytoplasmic or nuclear domains in both DMS114 EV and SOX2 GOF cells (Figs. 3E and 3F). Analogous to our RNA-FISH results (Figs. 3A), we observed that RMST is enriched in the cytoplasm in DMS114 EV cells but showed nuclear enrichment in SOX2 GOF cells, by fractionation qPCR (Figs. 3G and 3H). We also showed that ES3 levels remained unchanged with high cytoplasmic enrichment regardless of SOX2 levels, suggesting that the localization changes were specific to RMST (Figs. 3G and 3H). We validated that the ARM mutation does not affect SOX2 nuclear localization (Fig. 3I). This implies that RMST sequestration in the nucleus is due to a direct interaction with the SOX2 ARM domain. In addition, we

examined AHCY localization with WT and ARM mutant SOX2 expression (Fig. 3I). Interestingly, the SOX2 ARM mutant rescued the nuclear sequestration of AHCY seen in prior WT SOX2 expression experiments (Figs. 1D-1F, 3I). These data suggest that SOX2 sequesters RMST and AHCY in the nucleus through its RNA-binding ARM domain.

SOX2 reprograms the methionine cycle at the AHCY step through its RNA-binding domain

The primary role of cytoplasmic AHCY is in the methionine cycle (Fig. 4A) which generates SAM for modulating DNA, RNA and histone methylation [21]. We therefore examined how the SOX2-RMST-AHCY complex modulates this metabolic process. Since SOX2 is canonically a transcription factor, we first examined methionine cycle gene expression changes by performing RNA sequencing (RNA-seq) in the SOX2 GOF and control cell lines (Fig. 4B). Interestingly, despite there being a significant number of differentially expressed genes (Table S2), the methionine cycle genes were relatively unchanged with SOX2 expression (Figs. 4B and S4A). Therefore, SOX2 does not regulate the methionine cycle at the transcriptional level.

To identify possible metabolic alterations by SOX2, we performed metabolite profiling in the SOX2 GOF and control cell lines (Fig. 4C). Nearly 300 metabolites were detected in these cells (Table S3). Stirkingly, methionine cycle metabolites were significantly altered by SOX2 expression, with SAM in particular demonstrating significant downregulation (Figs. 4C, 4D and S4B). The methylation index, expressed as the ratio of SAM to SAH, was significantly decreased in SOX2 GOF cells (Fig. 4E). Interestingly, SAH levels are significantly higher with SOX2 expression, suggesting that the methionine cycle is being inhibited at the AHCY catalyzed step (Figs. 4A, 4C and 4D). This reduces the progression of the methionine cycle to generate SAM for methylation reactions, hence the significantly lower methylation index (Fig. 4E).

To further examine how SOX2 alters the methionine cycle, we repeated the metabolite profiling with SOX2 ARM mutant and SOX2 WT expression (Fig. 4F, Table S4). Interestingly, the SOX2 ARM mutant rescued the methionine cycle metabolite changes observed with SOX2 expression (Fig. 4F, 4G and S4C). The methylation index decrease was also reversed with the ARM mutant (Fig. 4H). Metabolite Set

Enrichment Analysis (MSEA) confirmed that methionine metabolism was one of the top 5 differentially altered pathways in both the SOX2 GOF and SOX2 ARM mutant rescue experiments (Figs. S4D and S4E). These findings suggest that SOX2 can reprogram the methionine cycle through its RNA-binding ARM domain. We propose that RNA-dependent SOX2 nuclear sequestration of AHCY suppresses the levels of cytoplasmic AHCY to advance the methionine cycle for SAM generation.

SOX2 induces DNA hypomethylation by lowering SAM levels

We demonstrated that SOX2 reprograms the methionine cycle to inhibit SAM production (Fig. 4C-4E), a vital precursor for methylation reactions. To identify the ramifications of this metabolic reprograming, we examined the effect of SOX2 expression on DNA methylation by whole genome bisulphite sequencing (WGBS). Intriguingly, WGBS analysis revealed significant global hypomethylation in SOX2 GOF and endogenous SOX2 hi cells compared to SOX2 lo controls (Figs. 5A-5C). To investigate if the observed DNA methylation changes altered gene expression, we generated lists of significantly differentially expressed (DE) genes and non-DE genes from our RNA-seq data (Fig. 4B, Table S2). Strikingly, the overall DNA methylation patterns of upregulated, downregulated, or unchanged genes similarly reflected a global hypomethylation status (Figs. S5A-S5C). This indicates low correlation between DNA methylation and gene expression changes in response to SOX2 expression. Interestingly, the levels of DNA methylation enzyme DNMT1 were also not altered with SOX2 expression (Fig. S5D), suggesting that the observed DNA hypomethylation is not due to a change in enzyme expression. We validated these observations with IF for DNA methylation mark 5-methylcytosine (5mC) and expectedly, observed that 5mC levels were significantly reduced in SOX2 hi endogenous and isogenic cell line models (Fig. 5D). Our data suggests that SOX2 induces global DNA hypomethylation in cancer cells.

DNA hypomethylation leads to genomic instability in cancer [37]. We therefore examined if SOX2 expression could lead to genomic instability by performing IF with γH2AX to visualize DNA breaks [38]. We observed significant nuclear γH2AX levels in

SOX2 hi and SOX2 GOF cells, with almost no detection in SOX2 lo controls (Fig. 5E). Centrosome dysfunction also contributes to genomic instability. Centrosome component pericentrin levels are increased in malignant cells which ultimately leads to cancer progression through genomic instability [39]. We therefore performed IF with pericentrin and expectedly observed higher levels in SOX2 hi and SOX2 GOF cells (Fig. 5F). To validate that SAM levels are responsible for the DNA methylation changes induced by SOX2 expression, we supplemented SOX2 hi and GOF cells with different SAM concentrations. We observed a dose-dependent increase of 5mC levels (Figs. 5G and 5H) and dose-dependent decrease in γH2AX levels (Figs. 5I and 5J) with SAM treatment. SAM supplementation therefore rescues the DNA hypomethylation effects of SOX2 expression. We also examined the effects on histone methylation as a possible ramification of SOX2 metabolic reprograming. However, no significant changes were detected in the levels of three histone methylation marks in SOX2 lo and SOX2 hi cell lines (Fig. S5E). Our data suggests that SOX2 induces DNA hypomethylation in cancer by lowering SAM levels.

SOX2 DNA hypomethylation effects are dependent on its RNA-binding domain

To examine the role of the SOX2-RMST-AHCY complex in DNA hypomethylation, we expressed ARM mutant SOX2 and assessed cellular 5mC and γH2AX levels by IF. Intriguingly, we found that similar to SAM supplementation (Fig. 5G and 5H), low 5mC levels induced by SOX2 were rescued by the SOX2 ARM mutant (Fig. 5K). Similarly, high γH2AX levels induced by SOX2 were rescued by the ARM mutant (Fig. 5L), just like with SAM supplementation (Figs. 5I and 5J). This data suggests that the SOX2-RMST-AHCY interaction plays a role in DNA hypomethylation.

SOX2-RMST-AHCY complex-driven DNA hypomethylation is evident in cancer patients

Our data thus far suggests that the SOX2-RMST-AHCY nuclear sequestration complex leads to global DNA hypomethylation in cancer cells. To validate these findings in human samples, we analysed 3 tumor resections from SCLC patients.

Through IF and RNA-FISH experiments, we observed co-localization of SOX2 with AHCY and RMST in SCLC tumors in the nucleus (Figs. 6A and 6B). In adjacent normal sections, AHCY and RMST were primarily present in the cytoplasm (Figs. 6A and 6B). We further observed that DNA methylation, as measured by 5mC, was clearly depleted in the SOX2 expressing tumors compared to adjacent normal tissues where SOX2 was absent (Fig. 6C). SOX2-expressing tumors also showed increased DNA damaged by nuclear γH2AX staining as compared to adjacent normal tissues (Fig. 6D). These findings in SCLC patient biopsies validate the clinical relevance of our findings that SOX2 sequesters RMST and AHCY in the nucleus, resulting in DNA hypomethylation and increased DNA damage.

SOX2-expressing cancer cells are sensitized to AHCY inhibition

Our data suggests that SOX2-RMST sequestration of AHCY inhibits methionine cycle-dependent SAM generation, a key process for cell survival. We therefore examined if SOX2-expressing cancer cells, with low SAM levels, would be sensitized to further AHCY inhibition. AHCY knockdown selectively reduced the cell viability of SOX2 hi and SOX GOF SCLC cells but not SOX2 lo cells (Figs. S6A and 7A-7D). Similarly, SOX2 hi HCC cells were more sensitive to AHCY knockdown as compared to SOX2 lo cells, which were unaffected (Figure 7E-7H). Cell proliferation, assessed by BrdU incorporation, was also reduced in the SOX2 GOF cells compared to the EV control upon AHCY knockdown (Figs. 7I and 7J). In addition, AHCY knockdown increased the levels of apoptotic cell death markers cleaved PARP1 and cleaved caspase 3, specifically in SOX2 hi H446 and SOX2 GOF cells, with minimal effect on SOX2 lo cells (Fig. 7K). Our results suggest that SOX2-expressing cancer cells are more dependent on AHCY for growth and survival.

Pharmacological inhibition of AHCY selectively targets SOX2-expressing cancer

Since SOX2-expressing cells are more dependent on AHCY activity for growth and survival, we wondered if pharmacological inhibition of AHCY could target SOX2 tumors *in vivo*. DZNep is a potent small molecule inhibitor of AHCY [40]. To test the efficacy of this drug in SOX2-expressing SCLC cells, we treated several SOX2 hi and lo SCLC and HCC cells, as well as lung fibroblast MRC5 cells as a control. SOX2 hi SCLC and HCC were particularly sensitive to DZNep treatment while SOX2 lo cells

and MRC5 were minimally affected (Fig. 7L and 7M). Next, we assessed if DZNep effects could be observed *in vivo*. We established two orthotopic SCLC xenograft models with SOX2 hi luciferase-expressing (Luc) cell lines, H446-Luc and H69-Luc, as well as an orthotopic SOX2 lo SW1271-Luc control. After significant tumor engraftment and growth, we administered vehicle or DZNep via intra-peritoneal (i.p.) injection. During the treatment period, mouse weights were roughly similar, suggesting minimal toxicity (Figs. 7N and S6B). Due to unknown circumstances, Luc expression of H69-Luc was lost during the experiment, so tumor sizes were examined after the full treatment duration allowed by our protocols. Strikingly, we observed a near complete disappearance of tumors in the SOX2 hi models (Figs. 7O and S6C-S6F). Conversely, SOX2 lo tumor growth was minimally affected (Figs. 7P and S6G). SOX2 hi H446 mice also demonstrated improved survival with drug treatment while the SOX2 lo SW1271 model showed no difference in survival, as all mice were sacrificed on the same day for displaying signs of suffering (Figs. S6H and S6I). As SOX2 hi H69-Luc mice lost their luciferase expression, all mice had to be sacrificed at the experimental end point to assess tumor size differences, hence survival differences could not be determined. Our data suggests that pharmacological AHCY inhibition can selectively target the vulnerable metabolic status of SOX2-expressing tumors.

Discussion

In this study, we developed an alternative strategy to identify protein complex compositions that depend on RNA, a proxy for functional RNA-protein interactions (Fig. 1A). Prior methods resulted in studies that primarily focused on the functions of one protein interacting with one or more RNAs. On the other hand, SPRINT allows for the identification of protein-protein interactions dependent on one or more RNAs. This perspective allowed us to identify a previously uncharacterized function of SOX2 in metabolic enzyme sequestration through a non-coding RNA RMST adaptor. Unlike other RNA-protein detection methods, we forgo the cross-linking step to minimize non-specific binding and simplify the protocol. Even without cross-linking, we detect significant RNA-dependent protein-protein interactions that are likely biologically relevant. Interestingly, we also identified SOX2 interactions with ribosomal proteins (Fig. 1C and Table S1), which hint at a SOX2-ribosome interaction. Since the ribosome is primarily composed of RNA, we can surmise that

RNase digestion in SPRINT would lead to ribosomal degradation, thereby resulting in the loss of SOX2-ribosomal protein interactions observed. Our SPRINT results therefore propose that SOX2 interacts directly with the ribosome, a finding which was recently independently published by another group[29]. This SOX2-ribosome study validates the utility of SPRINT in detecting biologically relevant interactions. We propose that SPRINT will be useful to robustly identify functional RNA-protein interactions across various biological fields.

The SOX2-RMST-AHCY complex identified by SPRINT likely reprograms the methionine cycle to induce DNA hypomethylation, a cancer hallmark. Our data suggests that SOX2 uses its TF-associated affinity for binding chromatin to sequester AHCY in the nucleus through RMST (Figs. 1D-I, 3, 6A, and 6B). Reducing the pool of AHCY in the cytosol, where the methionine cycle occurs in concert with other enzymes, likely disrupts the flow of metabolite precursors through the cycle. This reduces the production of cellular SAM, which is indispensable for methylation reactions [41]. In line with this hypothesis, we observed significant changes in methionine cycle metabolites, particularly at the AHCY catalyzed step, and methylation precursor SAM upon SOX2-expression (Figs. 4, S4B and S4C).

The reduction in SAM in cells with the SOX2-RMST-AHCY complex active likely leads to a lack of precursors for DNA methylation. Hence, the predicted outcome is global DNA hypomethylation, which causes genome instability [42]. This outcome is expectedly what we observed, with SOX2 GOF and SOX2 hi cancer cells and patient tumors demonstrating significantly lower levels of DNA methylation (Figs. 5A-5D, and 6C). This in turn leads to an increase in chromosomal instability, reflected by higher levels of gamma γH2AX and pericentrin in the SOX2-high cells and tumors (Figs. 5E, 5F, and 6D). Furthermore, we demonstrate that SAM supplementation and a SOX2 RNA-binding domain mutant can rescue the aforementioned epigenetic effects (Figs. 5G-5L). We therefore provide evidence that SOX2 can induce DNA hypomethylation with consequent chromosomal instability through lowering SAM levels. This activity is dependent on the ability of SOX2 to bind RNA. We also show that SOX2-expressing cells are dependent on RMST and AHCY for growth and survival in SCLC (Figs. 2D-2G and 7A-7D) and HCC (Figs. 2H-2K and 7E-7H) cells. This implies that both RMST and AHCY are required for SOX2-dependent cancer cell survival. Based on our data, it is likely that SOX2 amplification or overexpression in

cancer utilizes RMST to sequester AHCY in the nucleus, thereby inhibiting SAM production to induce DNA hypomethylation and chromosomal instability to drive tumorigenesis.

The SOX2-RMST-AHCY mechanism provides evidence for the functional role of RMST in cancer. LncRNAs are important genome regulators in cancer and play versatile roles in the cytoplasm and nucleus [43]. These lncRNAs interact with other proteins to cause chemoresistance [44,45], tumour suppression or promote tumour growth [46,47] and metastasis [48]. RMST has been shown to be involved in neural differentiation [16], but its role in cancer is unclear. We observed that RMST is highly enriched in SCLC and ovarian cancer, among others (Fig. 2O). Coincidentally, SOX2 is highly expressed in and has been shown to play important oncogenic roles in SCLC and ovarian cancer [49,50]. In this study, we demonstrate a functional role for RMST as an adaptor for SOX2 to sequester AHCY in the nucleus, thereby reprograming the methionine cycle in cancer. It could therefore be interesting to investigate if the SOX2-RMST-AHCY complex similarly contributes to tumorigenesis in other cancers.

Other than mechanistic insight, our work potentially defines a druggable metabolic vulnerability in SOX2-driven cancer. TFs represent a major class of protein that's frequently dysregulated in many cancers [51]. However, the vast majority of them remain undruggable [52]. Our work suggests that the SOX2-RMST-ACHY sequestration complex significantly reduces SAM to initiate DNA hypomethylation and chromosomal instability, which drives tumorigenesis. However, this could be a double-edged sword where SOX2-expressing cells become increasingly dependent on the remaining SAM for methylation reactions to survive. In addition, further genome-wide DNA hypomethylation could induce irreparable DNA damage that even cancer cells cannot withstand. Thus, inhibiting AHCY activity further could prove detrimental to the survival of these cancer cells. Indeed, applying for AHCY inhibitor DZNep resulted in potent activity against SOX2-expressing SCLC and HCC cells in culture and SCLC *in vivo* (Figs. 7 and S6). Interestingly, AHCY inhibition at higher doses did not significantly affect the cell viability of SOX2 lo SCLC and HCC cells, and a lung fibroblast cell line (Fig. 7L and 7M). AHCY inhibition also did not alter tumor growth of a SOX2 lo orthotopic xenograft despite potently reducing tumor burden in two SOX2 hi orthotopic xenografts (Figs. 7O-7P and S6C-S6G). Mouse models did not show significant signs of drug toxicity-induced weight loss

during drug treatment (Figs. 7N and S6B). This suggests that cells that do not express SOX2 can be spared during AHCY inhibition, resulting in a sufficient therapeutic window for targeting SOX2-expressing cancer cells. The methionine cycle is an essential metabolic process in all cells, so targeting this pathway could lead to significant side effects. On the contrary, our work suggests a targeted way to apply methionine cycle inhibitors, utilizing SOX2 expression as a biomarker, to achieve lower toxicity in SCLC and potentially other SOX2-expressing cancers. SCLC remains a cancer of unmet need, with a 6% 5-year survival rate [53]. The development of a new targeted therapy involving AHCY in SOX2-expressing tumors could therefore be transformative for SCLC and other cancer patients.

Collectively, our findings suggest a concerted TF-lncRNA-metabolic enzyme mechanism that reprograms metabolism but also induces a vulnerability in cancer. TFs like SOX2 have been shown to drive cancers primarily through transcriptional regulation [14]. In our work, we introduce a different paradigm where TFs coopt lncRNAs for non-canonical functions. This knowledge adds an additional dimension to how TFs function as oncogenes. Our study also highlights the possibility of discovering other adaptor functions of non-coding RNAs that bridge two seemingly incongruous processes. With a detailed understanding of the mechanism by which SOX2-RMST-AHCY induces metabolic reprograming, we hypothesized and validated a means to selectively target SOX2-driven cancer. This paves the way for the development of clinical inhibitors for AHCY and other methionine cycle enzymes in tandem with a SOX2 biomarker for precision therapy.

Methods

Cell lines

All cell lines were genotyped to confirm identity upon receipt and tested for mycoplasma contamination every 3 months. SCLC cells were grown in Gibco RPMI-1640, 10% FBS, 1% pen/strep, and 1% glutamine (Thermo Fisher Scientific). HCC cells were grown in Gibco DMEM, 10% FBS, 1% pen/strep, and 1% glutamine. Cell lines were cultured at 37°C with 5% CO_2. Transgenic SOX2 expressing cells were prepared by transducing pBABE SOX2 lentivirus into DMS114 for stable expression.

Lentiviral transduction

Lentivirus was produced in HEK293T cells. After 48 hrs, virus was collected and filtered through a syringe filter and added to the required cell line. 8 µg/ml polybrene was added to cells. After 48 hrs, puromycin selection was carried out.

Cell viability assay

Cells were plated in 96 well plates. After overnight incubation, cells were treated with DZNep serial dilution and incubated for 3 days. CellTitre-Glo (Promega) was performed according to manufacturer instructions. Luminescence signal was acquired using GLO MAX microplate reader (Promega). Data was analyzed using GraphPad prism software. For knockdown cell viability, after stable cell line construction, cells were plated in 96 well plates, and readings were taken for day 1, 3, 5, and 7.

Western blot

Western blot was performed as previously described [54]. Cell lysate was prepared in RIPA buffer (thermo fisher scientific) supplemented with protease and phosphostop (sigma Aldrich). Total protein concentration was measured by BCA protein kit (Beyotime). Equal amounts of protein were loaded in Sure PAGE (4-20%) pre-casted gels (Gene script), proteins were transferred to membrane by the quick semidry method (BioRAD). Membrane was blocked in quick block buffer (Beyotime) for 15 mins and incubated with primary antibodies overnight at 4°C followed by incubation with HRP conjugated antibodies the next day. Membrane was imaged using Chemidoc (BioRAD) and ECL reagent (Yamei).

Co-Immunoprecipitation/MS

Cell lysate was prepared in IP lysis buffer (Pierce) supplemented with protease inhibitor cocktail (Beyotime). After 30 mins, cell lysate was centrifuged for 15 mins at 13,000 rpm. Lysate was precleared with protein A/G beads (Dynabeads) for 2 hrs at 4°C with tumbling. 1% input was removed; lysate was incubated with antibodies for 4 hrs at 4°C. Antibodies and lysate were added to Dynabeads and rotated overnight at 4°C. The next day, beads were washed with IP lysis buffer and proteins were eluted in laemmli buffer. Western blot was performed as mentioned above. Samples were prepared for MS as previously published [55].Proteins were digested with 50 mM dithiothreitol and diluted in 50 mM Tris-HCl, pH 8.0 to reduce the urea concentration to 2 M. The lysate was digested overnight at 37°C on a shaker. 1% formic acid was added to acidify the peptides. Peptide desalting was performed using hypersep C18 cartridges (Thermo). Samples were dried by evaporation. MS samples were dissolved in 20 µl of ultrapure water + 0.1% formic acid.

RNA isolation and quantitative RT-qPCR

Total RNA was extracted by the RNeasy kit (Qiagen), and cDNA synthesis was performed using the revert aid CDNA synthesis kit (Thermo Fisher Scientific). Quantitative real time qPCR was performed using SYBR green (bimake.com) in triplicate in the CFX Connect Real-Time PCR Detection System (BioRAD). mRNA expression was quantified by the ΔΔCt method and normalized with either *ACTB* or *18S rRNA* for lncRNAs expression in SCLC.

Immunofluorescence

A modified protocol was used for IF staining. Cells were grown on cover slips. The next day, cells were fixed with 4% paraformaldehyde at room temperature (RT) for 15 mins, washed with PBS, permeabilized with 0.1% triton X-100 (BioRAD) for 5 mins at RT, and washed again with PBS three times, blocked with 5% BSA for 30 mins and incubated with primary antibodies at 4°C overnight. The next day, cells were washed with PBS and incubated with secondary antibodies for 1 hr at RT. Cells were washed with PBS, counter-stained with DAPI, and mounted on the slide with mounting media. Images were acquired with the LSM980 microscope (Zeiss). Qualification was performed with Image J software.

CUT&RUN qRT-PCR

CUT&RUN was performed as previously described [30]. Briefly, 3 × 10^6 H446, DMS114 EV, and DMS114 *Tg:SOX2* cells were collected. Cells were washed and resuspended in washing buffer (1M HEPES pH 7.5, 5M NaCl, 2M spermidine (Beyotime), protease inhibitor). 10µl of Concanavalin A beads (Beyotime) were washed twice with 1ml of binding buffer (1M HEPES-KOH, 1M KCL, 1M $CaCl_2$, 1M $MnCl_2$), then incubated for 10 mins at RT. After a brief spin, tubes were placed on a magnetic rack to remove the buffer. Cells were resuspended in 1ml digitonin washing buffer (washing buffer supplemented with 5% digitonin). The buffer was removed, then 50µl digitonin buffer containing primary antibody was added and the reaction was incubated overnight at 4°C with rotation. The next day after washing, pA-MNase (700ng/ml) in 50µl of digitonin buffer was added and the reaction was incubated for 10 mins at RT. Beads were washed twice with digitonin washing buffer, then resuspended in 100µl of wash buffer and incubated at 0°C in a heat block for 5 mins. 3µl of 100mM $CaCl_2$ was added to activate the pA-MNase and the reaction was incubated at 0°C for 30 mins. 100µl of stop buffer (5M NaCl, 0.5M EDTA, 0.2M EGTA, 5% digitonin, RNase A, 2mg/ml glycogen) was added followed by gentle mixing on a vortex, then incubation at 37°C for 10 mins to release CUT&RUN fragments. The reaction was centrifuged at 4°C for 5 mins at 16000 g and placed on a magnetic rack. The supernatant was transferred to a new tube and DNA was extracted via phenol chloroform extraction. qRT-PCR was performed as mentioned above.

BrdU assay

Cell death was examined by BrdU (Thermo Fisher Scientific) following the manufacturer's instructions. Cells were stained with labelling reaction at 37°C for 60 mins, fixed in 4% PFA, then permeabilized with 0.1% triton x-100 and 0.5N HCl. Cells were counter-stained with DAPI on slides. Images were acquired with the LSM980 microscope (Zeiss).

RIP-qPCR

RIP was performed as previously described [17] with little modification. We performed RIP under native conditions instead of UV cross-linking. 3µg SOX2 antibody was used to pull down RNA associated with SOX2 in cells. RNA was extracted via TRIzol method. Revert aid cDNA synthesis kit (Thermo Fisher Scientific) was used to synthesize cDNA with random primer. qPCR was run according to the aforementioned protocol.

Biotinylated RNA pull down

RNA pulldown assay was performed as previously described [56]. *In vitro* transcription of RMST with biotin labelling was performed with T7 RNA polymerase according to kit instructions (Beyotime). Cell lysate was prepared in RIP buffer (150mM KCl, 25mM Tris pH 7.4, 0.5mM DDT, 0.55% NP-40) with protease inhibitor and phosphostop (Roche). RNA loaded M-280 (Thermo Dynabeads) beads were incubated with precleared cell lysate at 4°C for 6 hrs. Next, beads were washed with RIP buffer 5 times and eluted in Laemmli buffer. Retrieved proteins were separated on WB gel as described above.

Fluorescence *in situ* hybridization (FISH)

RMST cDNA fluorescence labelled cy5 probes were purchased from Gene Script. Cells were plated on cover slips one day prior. FISH protocol was followed according to manufacturer's instructions (Beyotime). Cells were washed with PBS, fixed with 4% PFA and permeabilized with proteinase K for 5 mins at RT. Alkaline protein was neutralized by adding 0.5M HCl and washed with RNase free PBS. Neutralization of alkaline proteins by 0.5M HCl and acetylation of proteins by acetylation solution was performed for 5 mins to reduce the background and washed with PBS twice. Probe was diluted in hybridization buffer and added to cover slips for incubation in the dark for 2 hrs at 45°C. Wash cover slips with RNase-free PBS, counterstain with DAPI, then mount on slides with mounting media. Images were acquired with the LSM980 microscope (Zeiss).

Metabolomics

2.6×10^6 cells were collected, washed with PBS, then incubated with 80% pre-chilled methanol for 30 mins at -80°C. Lysate was collected in microfuge tubes and centrifuge for 10 mins at 4°C at 11,000 rpm. Supernatant was collected and air dried in a speed vac (Eppendorf). Samples were resuspended in distilled water for LC-MS/MS. Targeted metabolomics was performed in the 6500 QTRAP mass spectrometer (AB SCIEX, Framingham, MA, USA) with the previously described settings [57].

Orthotopic SCLC xenografts

Female NSG mice were purchased from GemPharmatech. Orthotopic lung tumours were grown as described previously [58]. 1.2×10^6 cells were implanted in lungs of mice by transverse incision in the left lateral thorax. Tumors grew up to one week and mice were randomly grouped into cages (6 mice per group). After sufficient tumor growth, DZNep or PBS were administrated twice a week on alternate days. Every week, luminescence signal was measured by the IVIS Spectrum (Perkin Elmer). Mouse experimental protocols were approved by the institutional animal care and use committee of Shenzhen Bay Laboratory.

Patients tissue specimen and fluorescence Immunohistochemistry (IHC)

Patients who participated in this study were diagnosed with SCLC and underwent surgery in the First Affiliated Hospital of Guangzhou Medical University. Biopsies collected were reviewed by pathologists to confirm SCLC diagnoses. Consecutive

4μm thick tissues were cut for IHC. Fluorescence IHC staining was performed according to Fun et al. [59]. Slides were dewaxed and rehydrated in fresh xylene 3 times, 100% ethanol, 95% ethanol, and 80% ethanol for 2 mins each. Antigen was retrieved in antigen retrieval buffer (Beyotime) for 20 mins in a microwave oven and cooled to room temperature. Slides were washed with PBS and permeabilized with 2% triton x-100. Tissues were blocked in BSA for 30 mins. Primary antibodies of AHCY, SOX2 5mC, gamma H2AX as well as RMST Cy5 probes were incubated at 37°C for 2 hrs. Samples were then washed with PBS 3 times for 3 mins each. The respective secondary antibodies were then incubated on tissues for 1 hr. at 37°C in the dark. Slides were counter-stained with DAPI, dehydrated and cover slipped. The stained slides were imaged with the LSM980 confocal microscope. Patient sample experimentation was approved by the ethics committee of the First Affiliated Hospital of Guangzhou Medical University.

Statistical information

CoIP/MS data analysis

CoIP/Mass data analysis was performed using Thermo Proteome Discover (version 2.5). Heatmap was generated with R package pheatmap. Co-IP data was clustered by complete linkage clustering with Euclidean distance.

WGBS analysis

WGBS analysis was performed similar to the previous study [60]. In short, the Illumina adaptor sequence and leading 10 bases were trimmed from paired-end reads by TrimGalore [61]. The trimmed sequences were mapped to human reference genome GRCh38 by BISMARK [62]. PCR duplicates were then removed by “deduplicate_bismark” command in the BISMARK package. From the M-bias plots, methylation bias was observed at the 5’ end in both reads. To remove the methylation bias, “--ignore 5 --ignore_r2 5” options were used during extraction of the DNA methylation status on every cytosine site with “bismark_methylation_extractor” command. To overcome the low sequencing depth in the data, the CpG methylation coverage status was merged from both strands and used for the downstream analysis. The global methylation status across the samples were compared by the R package, methylKit, with 10kb window size [63]. The partially methylated domains (PMDs) were identified by the “pmd” command in dnmtools [64]. The regional methylation profile plots were generated by “computeMatrix” and “plotProfile” command in deeptools [64].

RNA seq analysis

The paired-end RNA-seq reads were trimmed of adaptor sequences by *TrimGalore* and then mapped by STAR to the human reference genome GRCh38 with reference gene annotation GENCODE 45 [65]. Optical duplicates were marked and removed in the paired-end alignments by samtools with "-d 2500" option. Alignments with mapping quality < 20 were removed. Differentially expressed genes were identified using *DESeq2* [66], based on read counting results from the *Rsubread* package [67], with a fold change cutoff of 1 and a *q*-value cutoff of 0.05.

Data Availability

All information regarding cell lines, primers, probes and other resources is available in supplementary table S1-S7. Whole Genome Bisulphite Sequencing and RNA sequencing data is available through GEO accession number GSE285441 (token: erclueeezfsfzon). The mass spectrometry proteomics data have been deposited to the ProteomeXchange Consortium via the iProX partner repository with the dataset identifier PXD069283. Ms data can be accessed via https://www.iprox.cn/page/SSV024.html;url=1760795611345ezO9 with password x2Pl

References

1. Hentze, M. W., Castello, A., Schwarzl, T. & Preiss, T. A brave new world of RNA-binding proteins. *Nat Rev Mol Cell Biol* **19**, 327–341 (2018).
2. Khalil, A. M. & Rinn, J. L. RNA-protein interactions in human health and disease. *Semin Cell Dev Biol* **22**, 359–65 (2011).
3. Ramanathan, M., Porter, D. F. & Khavari, P. A. Methods to study RNA-protein interactions. *Nat Methods* **16**, 225–234 (2019).
4. Li, X., Song, J. & Yi, C. Genome-wide mapping of cellular protein-RNA interactions enabled by chemical crosslinking. *Genomics Proteomics Bioinformatics* **12**, 72–8 (2014).
5. Zheng, X. *et al.* Detecting RNA-Protein Interaction Using End-Labeled Biotinylated RNA Oligonucleotides and Immunoblotting. *Methods Mol Biol* **1421**, 35–44 (2016).
6. Nicholson, C. O., Friedersdorf, M. & Keene, J. D. Quantifying RNA binding sites transcriptome-wide using DO-RIP-seq. *Rna* **23**, 32–46 (2017).
7. Kim, S. Y. *et al.* The roles and mechanisms of coding and noncoding RNA variations in cancer. *Exp. Mol. Med.* **56**, 1909–1920 (2024).
8. Murphy, J. J., Surendranath, K. & Kanagaraj, R. RNA-Binding Proteins and Their Emerging Roles in Cancer: Beyond the Tip of the Iceberg. *Int. J. Mol. Sci.* **24**, 9612 (2023).
9. Huarte, M. *et al.* A large intergenic noncoding RNA induced by p53 mediates global gene repression in the p53 response. *Cell* **142**, 409–19 (2010).
10. Gupta, R. A. *et al.* Long non-coding RNA HOTAIR reprograms chromatin state to promote cancer metastasis. *Nature* **464**, 1071–6 (2010).
11. Tan, J. L. *et al.* Stress from Nucleotide Depletion Activates the Transcriptional Regulator HEXIM1 to Suppress Melanoma. *Mol Cell* **62**, 34–46 (2016).
12. Novak, D. *et al.* SOX2 in development and cancer biology. *Semin Cancer Biol* **67**, 74–82 (2020).
13. Schaefer, T. & Lengerke, C. SOX2 protein biochemistry in stemness, reprogramming, and cancer: the PI3K/AKT/SOX2 axis and beyond. *Oncogene* **39**, 278–292 (2020).
14. Weina, K. & Utikal, J. SOX2 and cancer: current research and its implications in the clinic. *Clin Transl Med* **3**, 19 (2014).

15. Holmes, Z. E. *et al.* The Sox2 transcription factor binds RNA. *Nat. Commun.* **11**, 1805 (2020).
16. Ng, S. Y., Bogu, G. K., Soh, B. S. & Stanton, L. W. The long noncoding RNA RMST interacts with SOX2 to regulate neurogenesis. *Mol Cell* **51**, 349–59 (2013).
17. Ng, S. Y., Johnson, R. & Stanton, L. W. Human long non-coding RNAs promote pluripotency and neuronal differentiation by association with chromatin modifiers and transcription factors. *Embo J* **31**, 522–33 (2012).
18. Sanderson, S. M., Gao, X., Dai, Z. & Locasale, J. W. Methionine metabolism in health and cancer: a nexus of diet and precision medicine. *Nat. Rev. Cancer* **19**, 625–637 (2019).
19. Mentch, S. J. *et al.* Histone Methylation Dynamics and Gene Regulation Occur through the Sensing of One-Carbon Metabolism. *Cell Metab.* **22**, 861–873 (2015).
20. Jin, X. *et al.* Unveiling the methionine cycle: a key metabolic signature and NR4A2 as a methionine-responsive oncogene in esophageal squamous cell carcinoma. *Cell Death Differ.* **31**, 558–573 (2024).
21. Vizán, P., Di Croce, L. & Aranda, S. Functional and Pathological Roles of AHCY. *Front Cell Dev Biol* **9**, (2021).
22. Lee, M.-S. *et al.* Ornithine aminotransferase supports polyamine synthesis in pancreatic cancer. *Nature* **616**, 339–347 (2023).
23. Wang, Z. *et al.* Methionine is a metabolic dependency of tumor-initiating cells. *Nat Med* **25**, 825–837 (2019).
24. Panatta, E. *et al.* Metabolic regulation by p53 prevents R-loop-associated genomic instability. *Cell Rep.* **41**, 111568 (2022).
25. Galatolo, D. *et al.* Bi-allelic mutations in HARS1 severely impair histidyl-tRNA synthetase expression and enzymatic activity causing a novel multisystem ataxic syndrome. *Hum Mutat* **41**, 1232–1237 (2020).
26. Ishii, K. *et al.* Characteristics and clustering of human ribosomal protein genes. *BMC Genomics* **7**, 37 (2006).
27. Uechi, T., Tanaka, T. & Kenmochi, N. A Complete Map of the Human Ribosomal Protein Genes: Assignment of 80 Genes to the Cytogenetic Map and Implications for Human Disorders. *Genomics* **72**, 223–230 (2001).
28. Dresios, J. *et al.* Cold stress-induced protein Rbm3 binds 60S ribosomal subunits, alters microRNA levels, and enhances global protein synthesis. *Proc Natl Acad Sci U A* **102**, 1865–70 (2005).
29. Schaefer, T. *et al.* Nuclear and cytosolic fractions of SOX2 synergize as transcriptional and translational co-regulators of cell fate. *Cell Rep.* **43**, 114807 (2024).
30. Skene, P. J., Henikoff, J. G. & Henikoff, S. Targeted in situ genome-wide profiling with high efficiency for low cell numbers. *Nat. Protoc.* **13**, 1006–1019 (2018).

31. Fu, Y. *et al.* LncRNA H19 interacts with S-adenosylhomocysteine hydrolase to regulate LINE-1 Methylation in human lung-derived cells exposed to Benzo[a]pyrene. *Chemosphere* **207**, 84–90 (2018).
32. Li, Q. *et al.* PVT1/miR-136/Sox2/UPF1 axis regulates the malignant phenotypes of endometrial cancer stem cells. *Cell Death Dis.* **14**, 177 (2023).
33. Teng, M. *et al.* Circular RMST cooperates with lineage-driving transcription factors to govern neuroendocrine transdifferentiation. *Cancer Cell* **43**, 891-904.e10 (2025).
34. Li, Z. *et al.* LncExpDB: an expression database of human long non-coding RNAs. *Nucleic Acids Res* **49**, D962-d968 (2021).
35. Oksuz, O. *et al.* Transcription factors interact with RNA to regulate genes. *Mol Cell* **83**, 2449-2463.e13 (2023).
36. Rahimi, K., Füchtbauer, A. C., Fathi, F., Mowla, S. J. & Füchtbauer, E.-M. Expression of the miR-302/367 microRNA cluster is regulated by a conserved long non-coding host-gene. *Sci. Rep.* **11**, 11115 (2021).
37. Daum, R., Brauchle, E. M., Berrio, D. A. C., Jurkowski, T. P. & Schenke-Layland, K. Non-invasive detection of DNA methylation states in carcinoma and pluripotent stem cells using Raman microspectroscopy and imaging. *Sci. Rep.* **9**, 7014 (2019).
38. Gantchev, J. *et al.* Tools used to assay genomic instability in cancers and cancer meiomitosis. *J Cell Commun Signal* **16**, 159–177 (2022).
39. Pihan, G. A. *et al.* Centrosome defects and genetic instability in malignant tumors. *Cancer Res* **58**, 3974–85 (1998).
40. Tseng, C. K. *et al.* Synthesis of 3-deazaneplanocin A, a powerful inhibitor of S-adenosylhomocysteine hydrolase with potent and selective in vitro and in vivo antiviral activities. *J Med Chem* **32**, 1442–6 (1989).
41. Shyh-Chang, N. *et al.* Influence of threonine metabolism on S-adenosylmethionine and histone methylation. *Science* **339**, 222–6 (2013).
42. Eden, A., Gaudet, F., Waghmare, A. & Jaenisch, R. Chromosomal Instability and Tumors Promoted by DNA Hypomethylation. *Science* **300**, 455–455 (2003).
43. Rinn, J. L. & Chang, H. Y. Genome Regulation by Long Noncoding RNAs. *Annu. Rev. Biochem.* **81**, 145–166 (2012).
44. Fang, S. *et al.* Long noncoding RNA-HOTAIR affects chemoresistance by regulating HOXA1 methylation in small cell lung cancer cells. *Lab Invest* **96**, 60–8 (2016).
45. Huang, W., Li, H., Yu, Q., Xiao, W. & Wang, D. O. LncRNA-mediated DNA methylation: an emerging mechanism in cancer and beyond. *J. Exp. Clin. Cancer Res.* **41**, 100 (2022).
46. Bao, X. *et al.* Knockdown of long non-coding RNA HOTAIR increases miR-454-3p by targeting Stat3 and Atg12 to inhibit chondrosarcoma growth. *Cell Death Dis* **8**, e2605 (2017).
47. Xiong, Y. *et al.* Long noncoding RNA HOXB13-AS1 regulates HOXB13 gene methylation by interacting with EZH2 in glioma. *Cancer Med* **7**, 4718–4728 (2018).

48. Zhang, C. *et al.* Long non-coding RNA Lnc-LALC facilitates colorectal cancer liver metastasis via epigenetically silencing LZTS1. *Cell Death Dis* **12**, 224 (2021).
49. Rudin, C. M. *et al.* Comprehensive genomic analysis identifies SOX2 as a frequently amplified gene in small-cell lung cancer. *Nat Genet* **44**, 1111–6 (2012).
50. Hellner, K. *et al.* Premalignant SOX2 overexpression in the fallopian tubes of ovarian cancer patients: Discovery and validation studies. *eBioMedicine* **10**, 137–149 (2016).
51. Lee, T. I. & Young, R. A. Transcriptional regulation and its misregulation in disease. *Cell* **152**, 1237–51 (2013).
52. Bushweller, J. H. Targeting transcription factors in cancer - from undruggable to reality. *Nat Rev Cancer* **19**, 611–624 (2019).
53. Rudin, C. M., Brambilla, E., Faivre-Finn, C. & Sage, J. Small-cell lung cancer. *Nat. Rev. Dis. Primer* **7**, 3 (2021).
54. Ishrat, I. *et al.* Development of a one-plasmid system to replace the endogenous protein with point mutation for post-translational modification studies. *Mol Biol Rep* **49**, 1–7 (2022).
55. Mertins, P. *et al.* Integrated proteomic analysis of post-translational modifications by serial enrichment. *Nat Methods* **10**, 634–7 (2013).
56. Tsai, M. C. *et al.* Long noncoding RNA as modular scaffold of histone modification complexes. *Science* **329**, 689–93 (2010).
57. Yuan, M., Breitkopf, S. B., Yang, X. & Asara, J. M. A positive/negative ion–switching, targeted mass spectrometry–based metabolomics platform for bodily fluids, cells, and fresh and fixed tissue. *Nat. Protoc.* **7**, 872–881 (2012).
58. Wilson, A. N., Chen, B., Liu, X., Kurie, J. M. & Kim, J. A Method for Orthotopic Transplantation of Lung Cancer in Mice. *Methods Mol Biol* **2374**, 231–242 (2022).
59. Fnu, T. *et al.* Sympathetic Neurons Promote Small Cell Lung Cancer through the β2-Adrenergic Receptor. *Cancer Discov.* **15**, 616–632 (2025).
60. Tan, H. K. *et al.* DNMT3B shapes the mCA landscape and regulates mCG for promoter bivalency in human embryonic stem cells. *Nucleic Acids Res* **47**, 7460–7475 (2019).
61. Felix Krueger, F. J., Phil Ewels, Ebrahim Afyounian, Michael Weinstein, Benjamin Schuster-Boeckler, Gert Hulselmans, &. sclamons. FelixKrueger/TrimGalore: v0.6.10 - add default decompression path (0.6.10). *Zenodo* https://doi.org/10.5281/zenodo.7598955 (2023) doi:10.5281/zenodo.7598955.
62. Krueger, F. & Andrews, S. R. Bismark: a flexible aligner and methylation caller for Bisulfite-Seq applications. *Bioinformatics* **27**, 1571–2 (2011).
63. Decato, B. E. *et al.* Characterization of universal features of partially methylated domains across tissues and species. *Epigenetics Chromatin* **13**, 39 (2020).

64. Ramírez, F., Dündar, F., Diehl, S., Grüning, B. A. & Manke, T. deepTools: a flexible platform for exploring deep-sequencing data. *Nucleic Acids Res* **42**, W187-91 (2014).
65. Dobin, A. *et al.* STAR: ultrafast universal RNA-seq aligner. *Bioinformatics* **29**, 15–21 (2013).
66. Love, M. I., Huber, W. & Anders, S. Moderated estimation of fold change and dispersion for RNA-seq data with DESeq2. *Genome Biol.* **15**, (2014).
67. Liao, Y., Smyth, G. K. & Shi, W. The R package Rsubread is easier, faster, cheaper and better for alignment and quantification of RNA sequencing reads. *Nucleic Acids Res.* **47**, e47–e47 (2019).
68. Labib, K., Tercero, J. A. & Diffley, J. F. Uninterrupted MCM2-7 function required for DNA replication fork progression. *Science* **288**, 1643–7 (2000).
69. Jayakumar, S. *et al.* PSIP1/LEDGF reduces R-loops at transcription sites to maintain genome integrity. *Nat. Commun.* **15**, 361 (2024).
70. Padavannil, A. *et al.* Importin-9 wraps around the H2A-H2B core to act as nuclear importer and histone chaperone. *Elife* **8**, (2019).
71. Champion-Arnaud, P. & Reed, R. The prespliceosome components SAP 49 and SAP 145 interact in a complex implicated in tethering U2 snRNP to the branch site. *Genes Dev* **8**, 1974–83 (1994).
72. Yang, Y. *et al.* PRPS1-mediated purine biosynthesis is critical for pluripotent stem cell survival and stemness. *Aging* **13**, 4063–4078 (2021).
73. Fararjeh, A. S. *et al.* Proteasome 26S Subunit, non-ATPase 3 (PSMD3) Regulates Breast Cancer by Stabilizing HER2 from Degradation. *Cancers Basel* **11**, (2019).
74. Choi, E.-B. *et al.* ATP-binding cassette protein ABCF1 couples transcription and genome surveillance in embryonic stem cells through low-complexity domain. *Sci. Adv.* **7**, eabk2775 (2021).
75. McCaul, N. & Braakman, I. Hold the fold: how delayed folding aids protein secretion. *Embo J* **41**, e112787 (2022).
76. Bialer, M. G. *et al.* MapB, the Brucella suis TamB homologue, is involved in cell envelope biogenesis, cell division and virulence. *Sci. Rep.* **9**, 2158 (2019).
77. Song, Z., Han, A. & Hu, B. Thymosin β4 promotes zebrafish Mauthner axon regeneration by facilitating actin polymerization through binding to G-actin. *BMC Biol.* **22**, 244 (2024).
78. Chapin, S. J. & Bulinski, J. C. Cellular microtubules heterogeneous in their content of microtubule-associated protein 4 (MAP4). *Cell Motil Cytoskelet.* **27**, 133–49 (1994).
79. Li, M. *et al.* Single symbiotic cell transcriptome sequencing of coral. *Genomics* **112**, 5305–5312 (2020).

Acknowledgements (optional)

We thank Zhi Han Lim, Yifan Hong, Zi Wang, Shiyuan Huang, the Multi-omics Mass Spectrometry Core, Bio-Imaging Core, and Laboratory Animal Centre of Shenzhen

Bay Laboratory for experimental assistance. We thank Dr. Chenqian Yin, Dr. Zhuobin Liang, Dr. Qin Peng, and Dr. Nanpeng Chen for providing reagents. We thank Dr. Leonard Zon and Dr. Yaoqi Zhou for manuscript feedback.

Ethics declarations

Patients tumor samples were collected by surgical operation at the First Affiliated Hospital of Guangzhou Medical University, China. Only resected samples from patients underwent surgery with written informed consent were included. This study was approved by the Ethics Committees of the First Affiliated Hospital of Guangzhou Medical University, China under ethics reference number: ES-2025-034-01

The animal study was approved by the experimental animal welfare ethics committee of Shenzhen Bay Laboratory. All animal experiments were strictly implemented in compliance with the IACUC Guide for the Care and Use of Laboratory Animals.

Competing interests

The authors declare no conflict of interest.

FUNDING

This research was supported by the Shenzhen Bay Laboratory Open Fund, SZBL2021080601003 (JLT); Shenzhen Bay Laboratory Proof of Concept Grant, S231801006 (JLT).

AUTHOR CONTRIBUTIONS

I.I and Z.I.B participated in methodology, data curation, investigation, and co-wrote the manuscript. Z.G. and H.K.H. participated in methodology, data curation, and investigation. R.M., Q.T., J.L., and Y.H., participated in data curation and investigation. L.Z., Y.H.W., N.J., and W.Y. provided supervision. H.K.T. provided supervision and participated in formal analysis. J.L.T. conceptualized the project, co-wrote the manuscript, and provided supervision and resources. All authors revised and approved the manuscript.

Figures

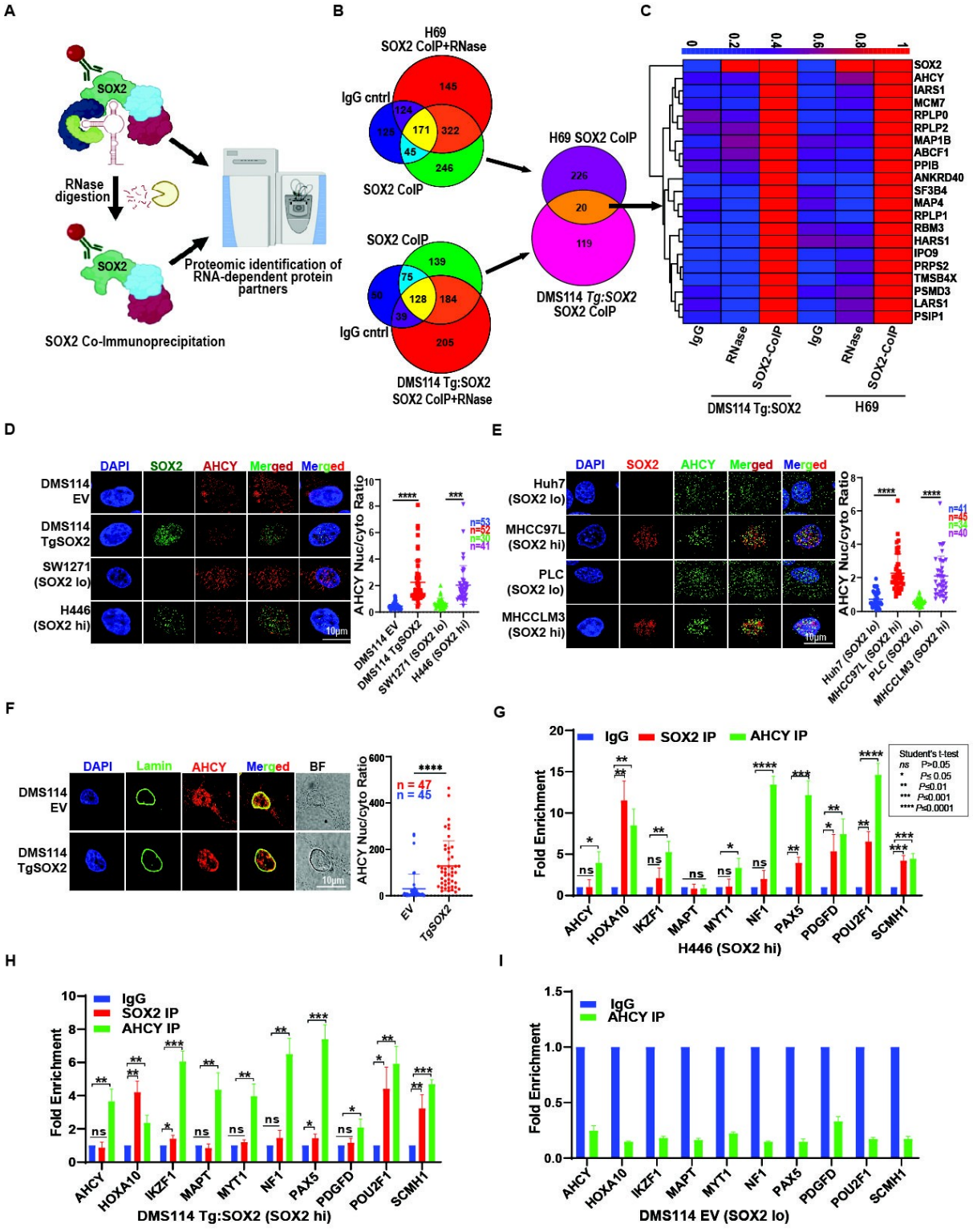

1005 **Fig. 1. SPRINT identifies AHCY as an RNA-dependent binder of SOX2 in cancer. (A)** Schematic of Surveying the Protein RNA-dependent Interactome (SPRINT) to identify novel RNA-dependent protein complexes. Created with

BioRender. **(B)** SPRINT was performed on endogenous SOX2-expressing SCLC cell line H69 and SOX2 gain of function (GOF) SCLC cell line DMS114 *Tg:SOX2*. Venn diagrams indicate the number of proteins identified via MS from the IgG pulldown control, SOX2 pulldown, and SOX2 pulldown with RNase treatment samples. Proteins that were uniquely detected in the SOX2 pulldown condition alone, indicating that they were specific SOX2 binders not found in the IgG pulldown, and below the detection cutoff in the RNase-treated condition, were shortlisted. Overlapping the shortlists from H69 and DMS114 *Tg:SOX2* experiments identified 20 proteins in common with reduced binding to SOX2 upon RNase treatment. **(C)** Heatmap indicating the relative protein levels for the 20 protein hits and SOX2 in the aforementioned SPRINT MS conditions, normalized to their individual levels in the SOX2 pulldown condition. Co-immunofluorescence (co-IF) of SOX2 and AHCY with DAPI as nuclear marker in SOX2 hi and lo **(D)** SCLC and **(E)** HCC cells. **(F)** IF of AHCY in DMS114 EV and DMS114 *Tg:SOX2* cells. DAPI and lamin staining delineate the nucleus and nuclear membrane respectively. Bright field (BF) images of cells are shown. For **(D-F)**, the ratio of nuclear to cytoplasmic AHCY signal was quantified per cell. CUT&RUN qRT-PCR of SOX2-bound gene promoter regions with IgG control, SOX2, and AHCY pulldown in **(G)** H446 hi SOX2, **(H)** DMS114 *Tg:SOX2*, and **(I)** DMS114 EV cells normalized to *ACTB*. Data is presented as mean ± SEM, n=3.

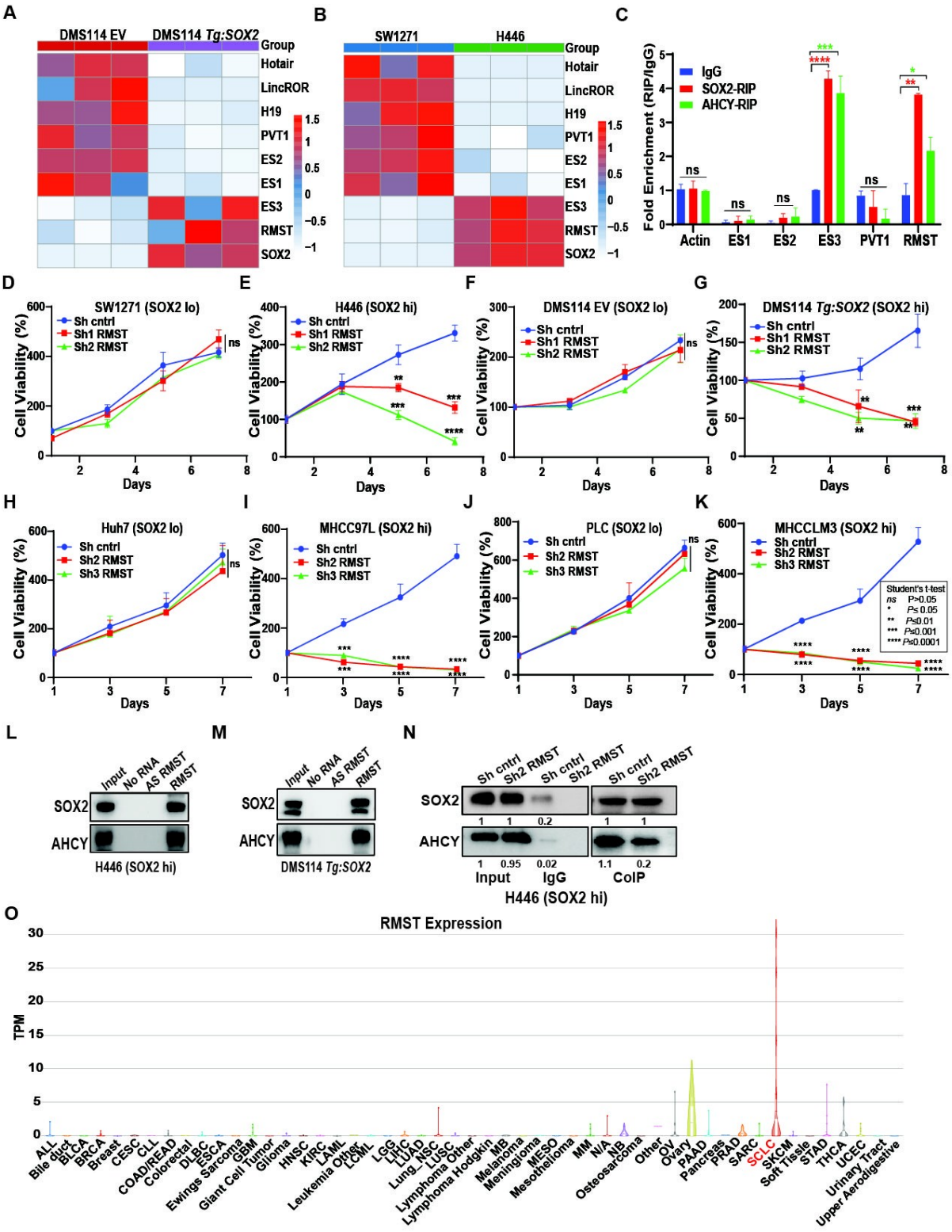

Fig. 2. The SOX2-AHCY interaction depends on lncRNA RMST. Heat map of qRT-PCR detection of candidate lncRNAs and *SOX2* in **(A)** isogenic cell lines DMS114 EV and DMS114 *Tg:SOX2* **(B)** endogenous cell lines SW1271, H446, normalized to *18S rRNA,* n=3. **(C)** Native RNA immunoprecipitation qPCR (RIP-

qPCR) was carried out on H446 cells. Conditions of IgG pulldown, SOX2 pulldown, and AHCY pulldown were analyzed for *ACTB*, *ES3* and *RMST* levels, n=3. CellTiter-Glo cell viability assay performed on **(D)** SW1271 (SOX2 lo), **(E)** H446 (SOX2 hi), **(F)** DMS114 EV, **(G)** DMS114 *Tg:SOX2*, **(H)** Huh7 (SOX2 lo), **(I)** MHCC97L (SOX2 hi), **(J)** PLC (SOX2 lo), and **(K)** MHCCLM3 (SOX2 hi) cells treated with scrambled control or shRNAs for *RMST* knockdown, n=3. **(L)** Western blot of SOX2 and AHCY with no RNA (streptavidin beads only) control, biotinylated RMST and antisense RMST pulldown in H446 and **(M)** DMS114 *Tg:SOX2* cells. **(N)** Co-immunoprecipitation (co-IP) of SOX2 with AHCY in the H446 cell line with scrambled control or *RMST* shRNA knockdown **(O)** *RMST* expression across multiple cancer cell types from LncExpDB. Statistical analysis was performed using Student's two-tailed t-test. Data is presented as mean ± SEM.

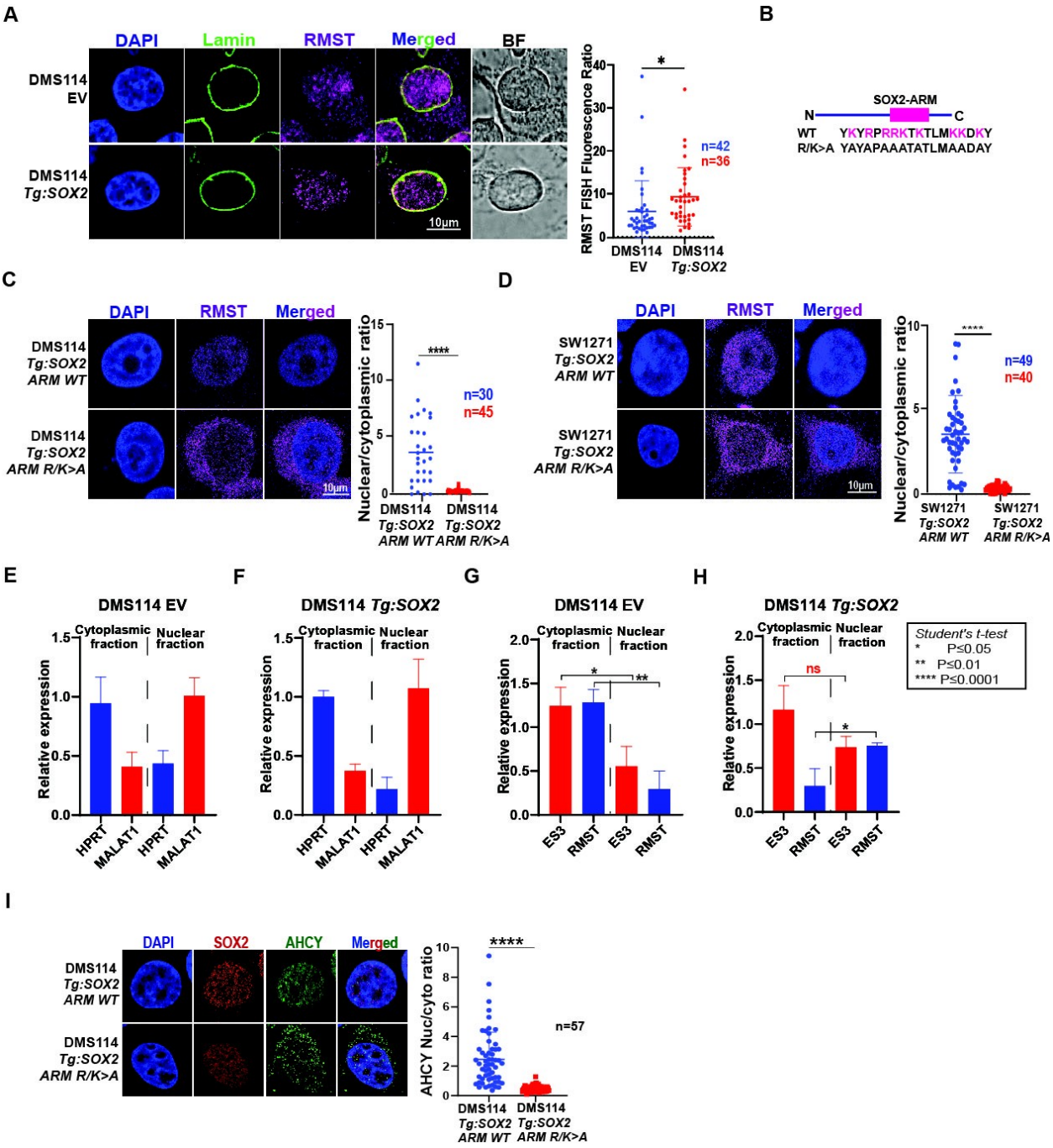

Fig. 3. SOX2 sequesters RMST and AHCY in the nucleus. (A) RNA fluorescent *in situ* hybridization (RNA-FISH) was performed with an *RMST* specific fluorescent probe on DMS114 EV and DMS114 *Tg:SOX2* cells. DAPI and lamin staining delineate the nucleus and nuclear membrane respectively. BF images of cells are shown. The ratio of nuclear to cytoplasmic *RMST* FISH signal was quantified per cell. **(B)** Visual representation of SOX2 wildtype and mutated RNA binding Arginine Rich motif (ARM). RNA-FISH was performed with an *RMST* specific fluorescent probe on **(C)** DMS114 *Tg:SOX2* and DMS114 *Tg:SOX2 ARM mutant* cells, and **(D)** SW1271 *Tg:SOX2 WT* and *Tg:SOX2 ARM mutant* cells with DAPI nuclear staining. **(E-H)** RT-

qPCR for various RNA species were performed on cytoplasmic and nuclear fractions of DMS114 EV and DMS114 *Tg:SOX2* cells, n=3. **(I)** Co-IF of SOX2 and AHCY with DAPI as nuclear marker in DMS114 *Tg:SOX2* and DMS114 *Tg:SOX2 ARM mutant* cells. For **(A**, **C**, **D** and **I)**, the ratio of nuclear to cytoplasmic RMST FISH and AHCY signal was quantified per cell. Statistical analysis was performed using Student's two tailed t-test. Data is presented as mean ± SEM.

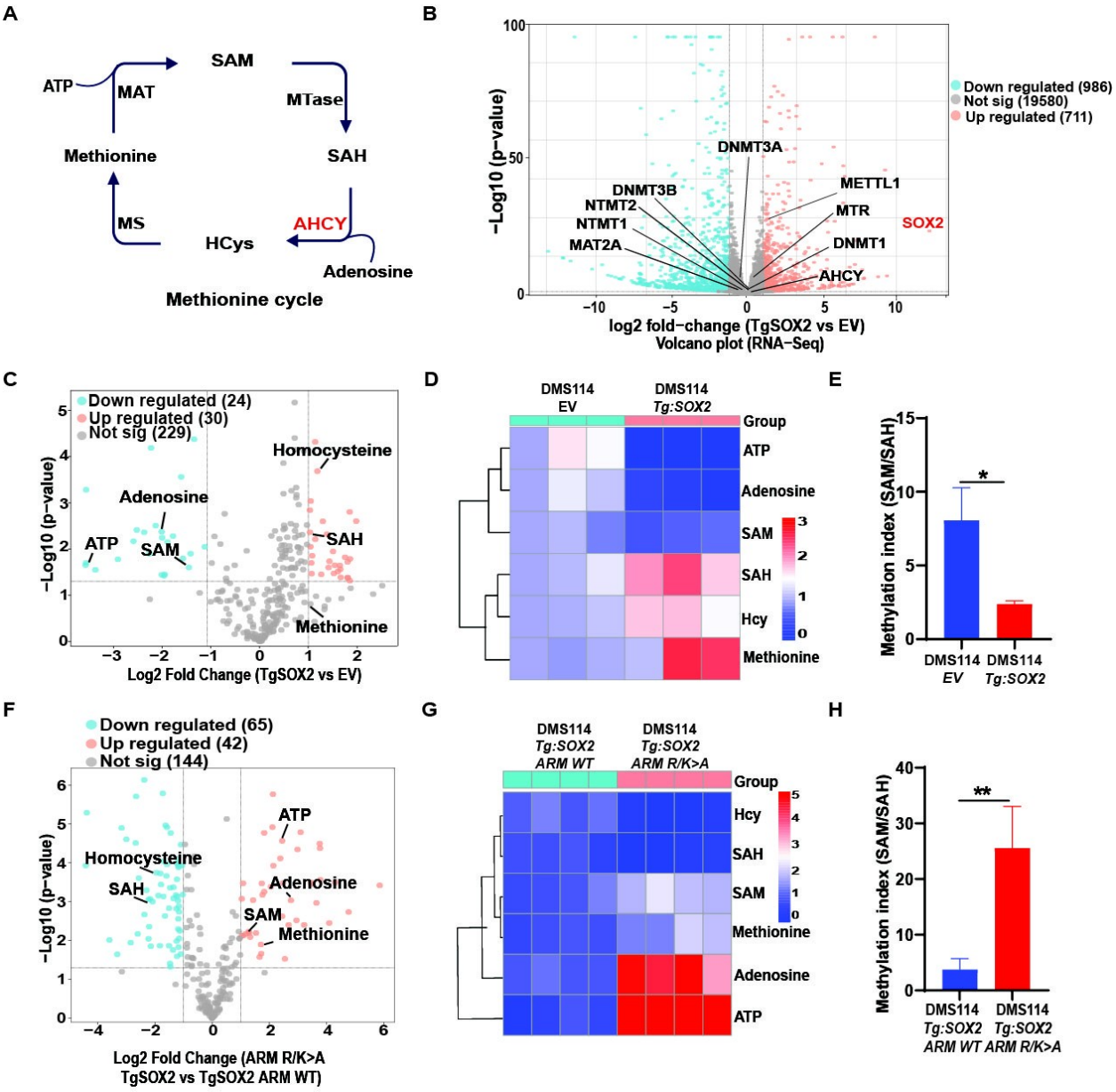

Fig. 4. SOX2 reprograms the methionine cycle through its RNA-binding domain. (A) Schematic of the methionine cycle. AHCY is highlighted in red. MAT: methionine adenosyltransferase; MTase; methyltransferase; MS: methionine synthase; ATP: adenosine triphosphate, SAM; S-adenosyl-L-methionine, SAH; S-adenosyl-L-homocysteine, HCys; homocysteine. **(B)** Volcano plot of RNA-seq data indicating fold changes in gene expression in DMS114 *Tg:SOX2* compared to DMS114 EV cells, highlighting methionine cycle genes. **(C)** Volcano plot of metabolite LC-MS/MS abundances normalized to cell number indicating folds changes in DMS114 *Tg:SOX2* compared to DMS114 EV cells, n=3. **(D)** Heatmap of methionine cycle metabolite abundances from the data in **(C)**. **(E)** Methylation index (SAM/SAH ratio) plot for DMS114 EV and DMS114 *Tg:SOX2* cells. **(F)** Volcano plot of metabolite LC-MS/MS abundances normalized to cell number indicating folds

changes in DMS114 *Tg:SOX2 ARM mutant* compared to DMS114 *Tg:SOX2* cells, n=4. **(G)** Heatmap of methionine cycle metabolite abundances from the data in **(F)**. **(H)** Methylation index (SAM/SAH ratio) plot for DMS114 *Tg:SOX2* and DMS114 *Tg:SOX2 ARM mutant* cells.

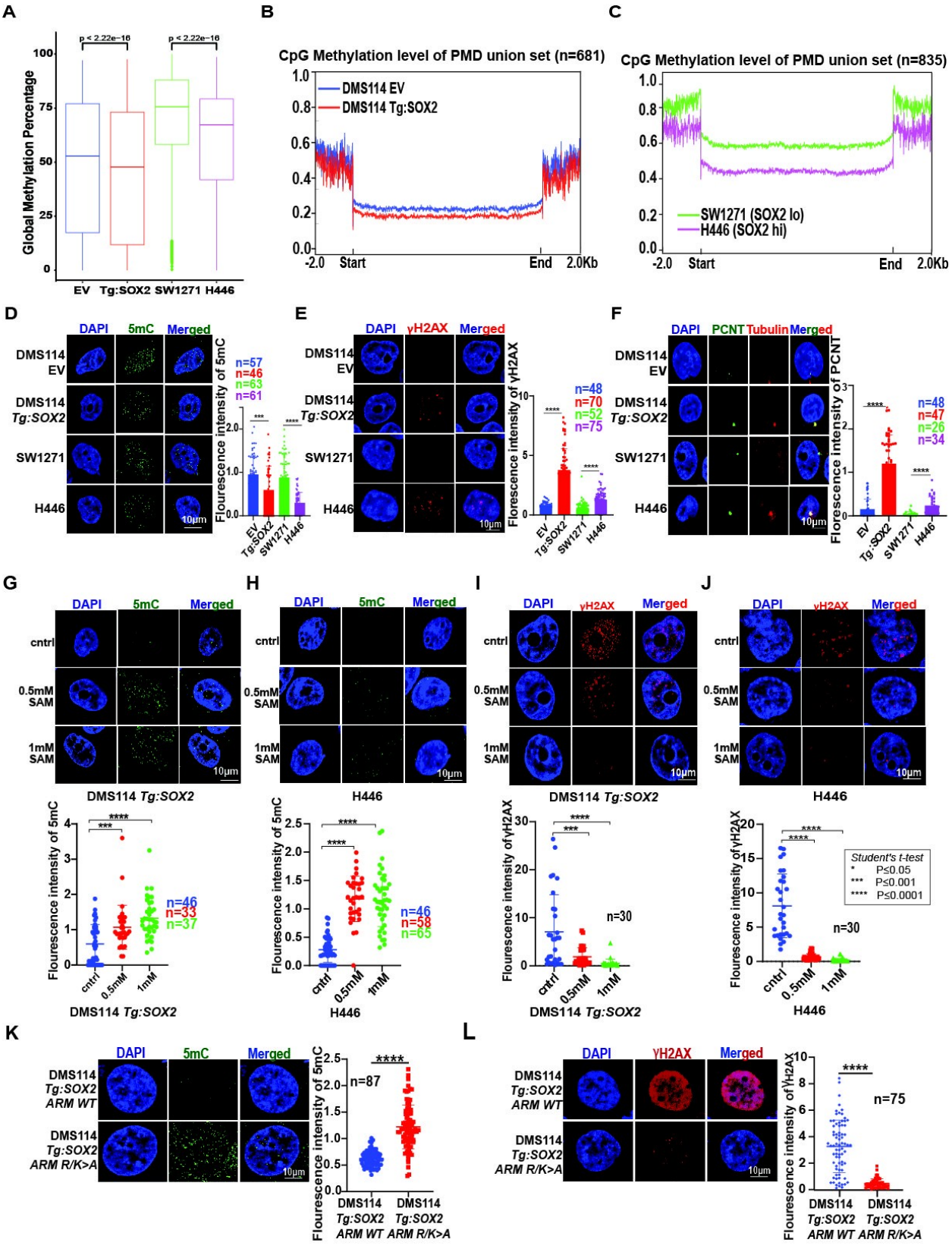

1080

Fig. 5. SOX induces DNA hypomethylation through its RNA-binding domain and lowering SAM levels. (A) Global CpG methylation percentage box plots of the cell lines in SCLC cell lines. Distribution of CpG methylation level of partially methylated domains (PMDs) from whole genome bisulfite sequencing performed on **(B)** DMS114 EV and DMS114 *Tg:SOX2*, and on **(C)** SW1271 (SOX2 lo) and H446 (SOX2 hi) cells. IF of **(D)** 5-methyl cytosine (5mC), **(E)** γH2AX, and **(F)** pericentrin in endogenous and isogenic SOX2 lo and hi SCLC cells. IF of 5mC after SAM treatment in **(G)** DMS114 *Tg:SOX2* and **(H)** H446 cells. IF of γH2AX after SAM treatment in **(I)** DMS114 *Tg:SOX2* and **(J)** H446 cells. IF of **(K)** 5-methyl cytosine (5mC) and **(L)** γH2AX in DMS114 *Tg:SOX2* and DMS114 *Tg:SOX2 ARM mutant* cells. For **(D-L)**, cells were stained with DAPI as a nuclear marker and IF signals were quantified per cell. Statistical analysis was performed using Student's two tailed t-test. Data is presented as mean ± SEM.

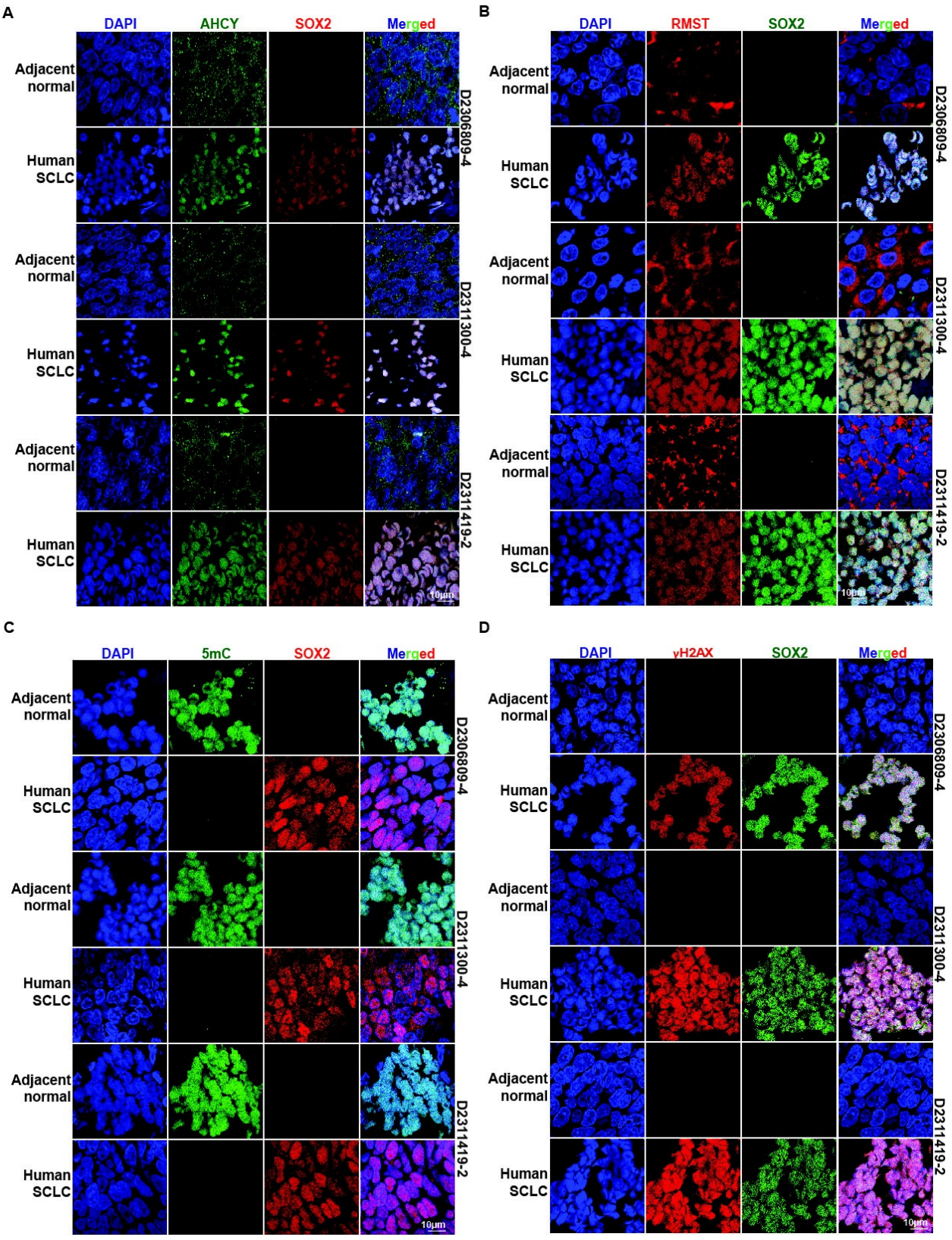

Fig. 6. RMST-conferred AHCY nuclear sequestration by SOX2 occurs in cancer patients. (A) Fluorescence immunohistochemistry (IHC) of AHCY, SOX2, and DAPI nuclear staining in three human SCLC patient samples and adjacent normal tissues. **(B**) RNA-FISH of *RMST* was performed in tandem with fluorescence IHC of SOX2 and DAPI nuclear staining in the same patient samples. Fluorescence IHC of **(C)** 5-methyl cytosine (5mC) and **(D)** γH2AX was performed in tandem with SOX2 fluorescence IHC and DAPI nuclear staining on the same patient samples.

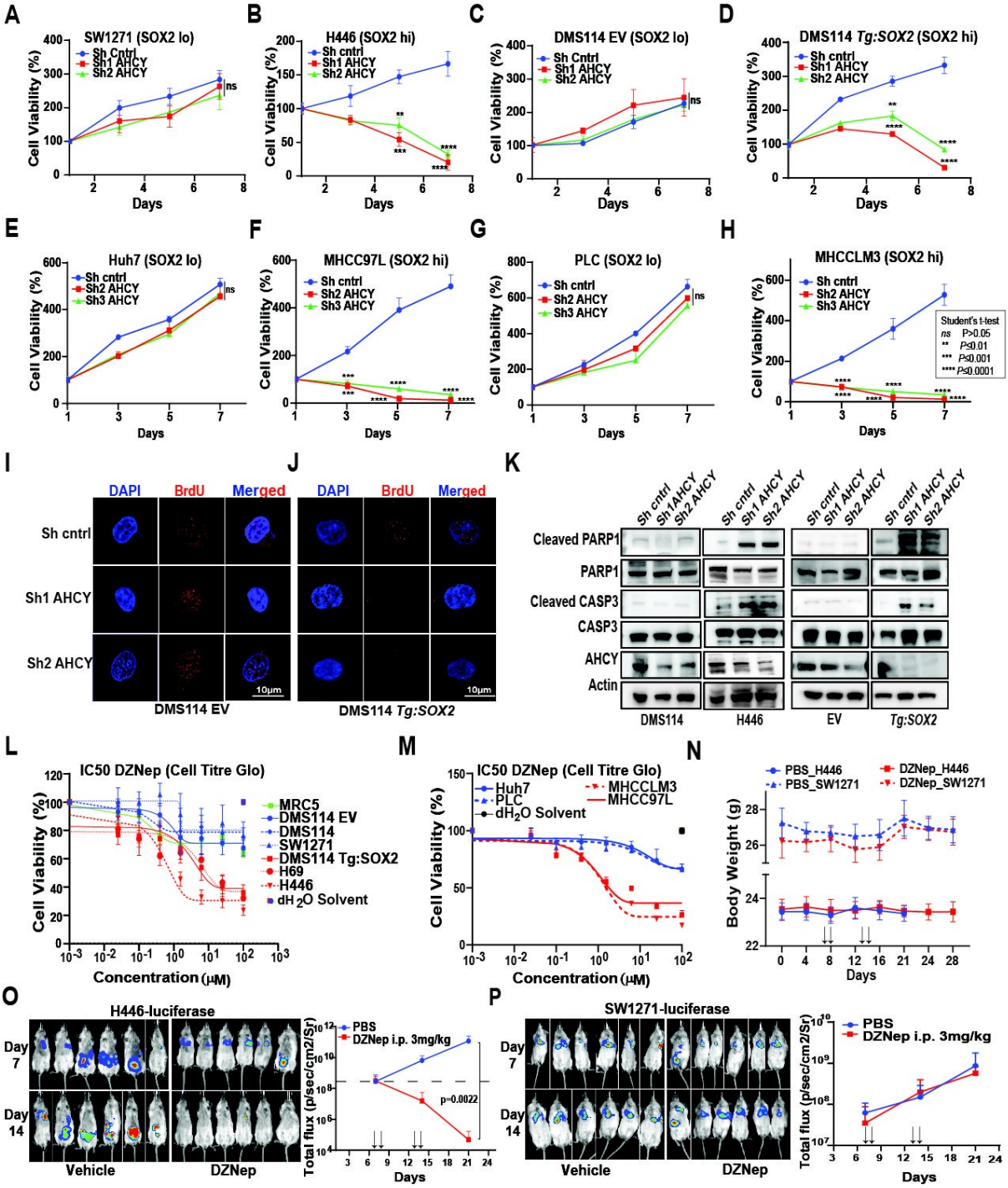

Fig. 7. SOX2-expressing cancer cells are sensitized to AHCY inhibition. CellTiter-Glo cell viability assay performed on endogenous SCLC cell line pair **(A)** SW1271 (SOX2 lo) and **(B)** H446 (SOX2 hi), isogenic SCLC cell line pair **(C)** DMS114 Empty Vector (EV) and **(D)** DMS114 *Tg:SOX2*, and endogenous HCC cell lines **(E)** Huh7 (SOX2 lo), **(F)** MHCC97L (SOX2 hi), **(G)** PLC (SOX2 lo), and **(H)** MHCCLM3 (SOX2 hi), treated with scrambled control or short hairpin RNAs (shRNAs) for *AHCY* knockdown, n=3. BrdU cell proliferation assay performed on **(I)** DMS114 EV and **(J)**

DMS114 *Tg:SOX2* cells treated with scrambled control or shRNAs for *AHCY* knockdown, n=3. **(K)** Western blot analysis of endogenous and isogenic SOX2 lo and hi SCLC cell lines treated with scrambled control or shRNAs for *AHCY* knockdown, with markers cleaved PARP1, PARP1, cleaved CASP3, CASP3, AHCY, and ACTB. CellTiter-Glo cell viability assay for **(L)** SOX2 lo and hi SCLC cell lines and lung fibroblast MRC5 cell line, and **(M)** SOX2 lo and hi HCC cell lines with DZNep treatment, n=3. **(N)** Body weights of orthotopic SCLC mouse models for SOX2 hi H446 and SOX2 lo SW1271 cells expressing luciferase (Luc), treated with intraperitoneal (i.p.) injection of phosphate buffer saline (PBS) or DZNep on days indicated by arrows, n=6. *In vivo* imaging and quantification of Luc activity luminescence signal in **(O)** H446-Luc and **(P)** SW1271-Luc orthotopic SCLC mouse models. Statistical analysis was performed using Student's two tailed t-test. Data is presented as mean ± SEM.